Aus der Abteilung für Vaskuläre Biologie und Tumorangiogenese
der Medizinischen Fakultät Mannheim
European Center for Angioscience (ECAS)
Direktor: Prof. Dr. med. vet. Hellmut Augustin

Characterization of the retinal neurovascular unit in zebrafish

Inauguraldissertation
zur Erlangung des medizinischen Doktorgrades
der
Medizinischen Fakultät Mannheim
der Ruprecht-Karls-Universität
zu
Heidelberg

vorgelegt von
Chiara Simone Middel

aus
Darmstadt
2022

Dekan: Prof. Dr. med. Sergij Goerdt
Referent: Prof. Dr. Jens Kroll

TABLE OF CONTENTS

Page

ABBREVIATIONS

°C	degrees Celsius
cm	centimetres
dpf	days post fertilization
g	grams
G	Gauge
h	hour
hpf	hours post fertilization
ml	millilitres
mm	millimetres
mpf	months post fertilization
No.	number
V	volt
W	watt
µl	microlitres

BBB	blood-brain barrier
BRB	blood-retinal barrier
BSA	bovine serum albumin
CNS	central nervous system
DAB	3'-3'-diaminobenzidine
DKA	diabetic ketoacidosis
DNA	deoxyribonucleic acid
DM	diabetes mellitus
DR	diabetic retinopathy
EC	endothelial cell
EGFP	endothelial green fluorescent protein
GC	ganglion cell
GCL	ganglion cell layer
GDM	gestational diabetes mellitus
GFAP	glial fibrillary acidic protein
GFP	green fluorescent protein
GS	glutamine synthetase
GWAS	genome-wide association studies
HHS	hyperglycaemic hyperosmolar state
HRP	horseradish peroxidase
IDF	International Diabetes Foundation
IHC	immunohistochemistry
ILM	inner limiting membrane
INL	inner nuclear layer
IOC	inner optic circle
IPL	inner plexiform layer
MODY	Maturity-onset diabetes of the young
NG2	neuron-glial antigen 2
NOD mouse	non-obese diabetic mouse
NPC	neuronal progenitor cell
NPDR	non-proliferative diabetic retinopathy
NVU	neurovascular unit

OIR	oxygen-induced retinopathy
ONL	outer nuclear layer
PAS	periodic-acid Schiff's
PAP	peroxidase-antiperoxidase
PBS	phosphate-buffered saline
PC	pericyte
PCNA	proliferating cell nuclear antigen
PCR	polymerase chain reaction
PDGFRβ	platelet derived growth factor receptor β
PDR	proliferative diabetic retinopathy
PTU	1-phenyl-2-thiourea
RDN	retinal diabetic neuropathy
RPE	retinal pigment epithelium
STZ	streptozotocin
TBST	Tris-Buffered Saline, 0.1% Tween® 20 detergent
TGF	transforming growth factor
TR	total retina
T1DM	type 1 diabetes mellitus
T2DM	type 2 diabetes mellitus
UKPDS	UK Prospective Diabetes Study
VEGF	vascular endothelial growth factor
vMC	vascular mural cells

1 INTRODUCTION

Parts of the chapters are part of the following publication and have been originally written by me.
Advancing Diabetic Retinopathy Research: Analysis of the Neurovascular Unit in Zebrafish
Chiara Simone Middel, Hans-Peter Hammes, Jens Kroll

The publication has been peer-reviewed and published in an issue of *Cells* (2021).

1.1 Diabetes mellitus

Diabetes mellitus is one of the most prevalent metabolic conditions in patients worldwide. The International Diabetes Foundation (IDF) estimated in 2015 that there were 415 million adults aged 20-79 living with diabetes. The study found that this number is expected to rise to 642 million people by 2040[1].
The majority of cases can be sorted into two different types, type 1 diabetes mellitus (T1DM, 5-10% of cases) and type 2 diabetes mellitus (T2DM, 90-95% of cases)[2]. T1DM is an autoimmune disease, in which the pancreatic β-cells are destroyed, decreasing the patient's ability to produce and secrete insulin and leading to absolute insulin deficiency. This type usually occurs in young patients and can only be treated by external insulin substitution[2]. The underlying pathogenesis in T2DM is the development of peripheral insulin resistance and therefore a relative insulin deficiency[2]. The number of people diagnosed with diabetes has increased dramatically in recent decades due to changes in the human environment and lifestyle which have resulted in increasing rates of obesity and other risk factors such as metabolic syndrome[3].
There are various other forms of diabetes as well, such as gestational diabetes mellitus (GDM), which is a form of glucose intolerance which first appears during pregnancy and usually resolves itself after delivery, and the different types of maturity-onset diabetes of the young (MODY), which are associated with monogenetic defects in β-cell dysfunction[2].
Diabetes is associated with multiple severe complications. Acute metabolic complications include diabetic ketoacidosis (DKA), the hyperglycaemic hyperosmolar state (HHS), lactic acidosis and conditions of hypoglycaemia which may result in coma[4, 5]. These acute complications can usually be prevented by treatment of the disease; however, they currently still account for high morbidity and mortality among patients with diabetes[5].
Long-term complications associated with diabetes include macro- and microvascular complications. Cardiovascular disease is associated with diabetes and a major cause of death and disability among patients with diabetes[5]. Microvascular complications include lower extremity amputations due to damage to the small vessels and the nervous system, diabetic neuropathy, diabetic nephropathy leading to end-stage renal disease and diabetic retinopathy[5].

1.2 Diabetic retinopathy

Diabetic retinopathy (DR) remains one of the leading causes of blindness or vision loss in the working age population worldwide[6].

The clinical aspects of DR have been well described[7-9]. The early steps in the pathogenesis of DR have been studied extensively, utilising various preclinical animal models as early human retinal samples are not available. A constant exposure to high levels of blood glucose leads to the formation of reactive oxygen species (ROS) which damage the cellular components of the retinal vasculature. The first apparent lesion is the loss of pericytes, a specialized kind of vascular mural cell, followed by the loss of endothelial cells, leaving acellular capillaries. As the acellular capillaries are incapable of providing sufficient blood flow to the retina, the retina becomes ischemic and secrets growth factors such as vascular endothelial growth factor (VEGF) and angiopoietin (Ang-)2[10].
In diabetic patients, characteristic early changes in the retina include altered blood flow and increased vascular permeability. Pericyte loss and formation of acellular capillaries contribute to the first clinically visible signs of non-proliferative DR (NPDR): microaneurysms, venous beading and intraretinal microvascular abnormalities[7, 11]. During moderate stages there are additional vascular abnormalities, most importantly intraretinal neovascularization. During later stages, due to increasing ischemia, retinal neovascularization extends through the inner limiting membrane (ILM) and along the surface of the retina or into the vitreous cavity. This stage is referred to as proliferative diabetic retinopathy (PDR) and can cause vision loss due to complications associated with the fragile new vessels which may lead to vitreous haemorrhage or retinal detachment[7]. Diabetic macular oedema (DME) develops because of the increased capillary permeability. This extracellular fluid can accumulate in the macular tissue and lead to vision loss due to macular detachment[7, 12]. Furthermore, recent studies have shown that the retinal pigment epithelium (RPE) may also be involved in the development of retinal pathologies. It is part of the outer blood retinal barrier (BRB) and controls the exchange of metabolites between the photoreceptors and the choroid vessels. Increased permeability may therefore lead to photoreceptor dysfunction[7, 13].
It was shown that development of DR can be prevented or delayed through intensive glycaemia treatment, intensive dyslipidaemia therapy and intensive blood-pressure therapy[14]. However, the UK Prospective Diabetes Study (UKPDS) showed that at the turn of the century, 38% of newly diagnosed patients with type 2 diabetes already showed some stage of retinopathy[15]. In a large European population-based study published in 2016, 21% of patients with screening-detected type 2 diabetes already showed signs of DR[16]. Further elucidation of the disease aetiology is therefore still needed to identify biomarkers, cytokines, factors or genes that mediate the disease progression and may be additional targets to treat DR[7].

1.3 Animal models of diabetic retinopathy

To understand the aetiology and pathogenesis of DR and to develop new treatment options, it is necessary to use animal models that represent the pathologies associated with DR in humans as closely as possible. There are various animal models of diabetes that are being used to study DR. Dog models of DR seem to have the most similar retinal morphological lesions to humans[17]. The most studied animal models are rodent models due to their small size, short life span and fast reproduction rate[18].
Diabetic animal models are developed in multiple ways, including overfeeding, pancreatectomy, destruction of β-cells and genetic mutation[18].
Streptozotocin (STZ) is the drug most used for induction of an insulinopenic type 1 diabetes. STZ was first isolated from *Streptomyces achromogenes* and proved to be an antibiotic with diabetogenic properties through the destruction of pancreatic β-cells[19]. The destruction of the β-cells leads to an inability to produce insulin and thereby

to a type 1 diabetes like state[19]. Various protocols for STZ induction of diabetes have been developed and hyperglycaemia usually occurs within 2 weeks after delivery of the first dose[18]. In STZ induced mice, DR phenotypes include gliosis 4-5 week after onset of hyperglycaemia[20], signs of neurodegeneration like retinal inner nuclear layer (INL) and outer nuclear layer (ONL) thinning[21] and acellular capillaries and pericyte ghosts after 6 months[20]. STZ can be used to induce diabetes in other animal models as well, including zebrafish[22].
High-sugar diets are a promising way of inducing diabetes in animal models as well. In rodents, the galactosemia models, whose diet contains 30-50% galactose, develop pathologies associated with early stages of DR including pericyte loss and acellular capillaries[23]. Immersion of zebrafish in alternating high-glucose solution leads to morphological changes in the retina in the form of significant inner plexiform layer (IPL) and INL thinning[24].
There are various genetic models of DR as well. The $Ins2^{Akita}$ mouse, which has a missense mutation in the *Insulin 2* gene leading to a conformational change in the insulin protein, protein accumulation in the β-cells and consequently β-cell death, is a frequently used model[25]. Another commonly used model is the non-obese diabetic (NOD) mouse. In NOD mice, $CD4^+$ and $CD8^+$ cells attack pancreatic β-cells, leading to their destruction and the impairment of insulin production. The NOD mouse is a polygenic model with at least three recessive genes contributing to diabetes development[26].
A genetic model to study type 2 diabetes is the db/db mouse. Animals with the homozygous mutation exhibit chronic hyperglycaemia, obesity and eventually atrophy of β-cells leading to hypoinsulinaemia[27]. There are multiple genetic rat models of DR as well, further demonstrating the complexity of genes associated with DR[18].
Early changes in the retina of diabetic animal models develop over the course of months. The first pathologies are a transient break down of the blood-retinal barrier (BRB) and the beginning of neuroglial cell apoptosis, followed by pericyte loss and activation of microglia and Müller glia. After six months of a diabetic metabolic state, neurodegeneration and vasoregression begin to occur. Longer lived mammalian models such as dogs or primates develop lesions such as microaneurysms, retinal macular oedema and intra-retinal neovascularization as well[28]. The continued need for various hyperglycaemic mammalian models is because each individual model, those mentioned above and those reviewed elsewhere[18, 23], only shows certain aspects of DR.
To induce pre-retinal neovascularization as in human PDR, the animal model of choice is the mouse oxygen-induced retinopathy model (OIR)[29]. While this model was highly important in the development of one of the main current therapies of neovascularization (anti-VEGF treatment)[30], in DR research it would be an advantage to have a model for neovascularization due to hyperglycaemia rather than hypoxia. One possible model is the homozygous *pdx1* knockout zebrafish, in which neovascularization was observed due to hyperglycaemia[31], making it a highly interesting model for DR research.

1.4 The neurovascular unit and its importance in diabetic retinopathy

Even though neurodegenerative changes have already been described in 1962[32], for a long time, both clinical studies and studies using animal models of DR focused mainly on the vascular dysfunctions associated with DR, such as pericyte loss, thickening of the basement membrane and endothelial cell dysfunction. Only in the late 1990s, researchers started broadening their perspective on the disease and taking a closer look at the neuroretina and the glial cells of the retina as well[33-35]. It was found that especially retinal ganglion cells and Müller glia are damaged in the retina of diabetic rats[33]

and that there was evidence of increased apoptosis in neural cells in both the retinae of diabetic rats and of diabetic donors[34, 36].
Neural and vascular cells are closely connected; this tight interaction has been characterized by the term “neurovascular unit” (NVU). Especially in the central nervous system (CNS) it is of vital importance that the transport of metabolites and nutrients as well as neurotransmitters is tightly regulated. The term NVU was first applied to the blood-brain barrier (BBB)[37, 38] and it was later adapted to the blood-retinal barrier (BRB) as well[39]. It describes this intricate functional and structural coupling of vascular cells, i.e., endothelial cells and vascular mural cells (especially pericytes), neural cells, which in the retina encompass ganglion cells, amacrine cells, horizontal cells, and bipolar cells as well as macro- (specifically Müller glia and astrocytes) and microglia.
The relevance of the NVU in the pathogenesis of DR has been studied extensively. The cells of the NVU in the retina work closely together to regulate blood flow through the retinal vessels. Physiologically, flickering light stimulates retinal blood vessels to dilate, while breathing 100% oxygen stimulates them to constrict due to the interaction of the different cells of the NVU. It was shown in various studies that in diabetic patients these responses are impaired before the first ophthalmological or clinical signs of DR become visible[40, 41]. Therefore, it is necessary to analyse the various components of the retinal NVU and identify how they get disrupted by diabetes.
As DR research focused exclusively on microvascular changes in the past, vascular endothelial cells emerged as the only therapeutic target. In diabetic conditions, VEGF levels are elevated which leads to increased blood vessel permeability and neovascularization[42]. Numerous retinal cells synthesize VEGF, including Müller cells, glial cells, ganglion cells, endothelial cells and pericytes[42]. Expression of the VEGF gene can be upregulated due to changes in glucose levels[43], formation of advanced glycation end products (AGEs) and hypoxia-inducible factor 1α (HIF-1α) activation through accumulating AGEs[44]. Furthermore, vascular cell interaction is impaired by diabetes. Pericytes both increase the vasculature’s susceptibility to VEGF signalling and control the expression of VEGF and Angiopoietin-2 (Ang-2) in endothelial cells with pericyte loss promoting VEGF signalling[45]. Pericyte loss and diabetic vasculopathy are further promoted by chronic hyperglycaemia through reduction of PDGF receptor tyrosine kinase signalling[46]. To prevent pathologies associated with increased levels of VEGF in the retina, intravitreal injections of VEGF-antibodies have been developed, successfully reducing vision loss and improving rates of vision gain in patients with DME[47].
However, all other components of the neurovascular unit are disrupted by diabetes as well, as multiple studies have shown. Typical signs of neuronal degeneration, which include diminished retinal neuronal function and neural-cell apoptosis have even been observed before the first signs of microvasculopathy are visible[34]. The first cell types that are affected by diabetes-induced apoptosis are photoreceptors, amacrine cells and retinal ganglion cells. The structural and functional consequences of this neural cells loss are reduced thickness of retinal layers and changes in electroretinography (ERG) results[48]. Glial activation (reactive gliosis), which is visible through upregulation of glial fibrillary acidic protein (GFAP) and associated with increased expression of VEGF in Müller cells, can play a role in damaging the retinal neurons and may be the link between the microvascular pathologies and the neurodegenerative process[49]. Additionally, microglia, the resident immune cells in the CNS, become activated. Physiologically, microglia protect the neuroretina from cell death and mediate regeneration, however, chronic activation due to hyperglycaemia may cause secondary tissue damage through constant pro-inflammatory stimuly[50].
In summary, all components of the NVU are in close contact and interact with each other. For a long time, the main pathologies associated with DR were microvascular

changes, as they are the first ones to become ophthalmologically visible. Multiple studies since have shown that neurodegenerative and inflammatory processes may precede microvasculopathy. As the current treatment options for DR mainly target vascular pathologies (anti-VEGF therapy and panretinal coagulation), animal models of DR are used to identify potential new therapeutic targets within the NVU.

1.5 Zebrafish as a model organism of diabetic retinopathy

Zebrafish *(Danio rerio)* have become a valuable vertebrate model to study various diseases and pathologies, including diabetes[51]. There are several features which have contributed to their current prominence, including their size (adult zebrafish are approximately 2.5 cm long), ease of maintenance and reproduction rate. Zebrafish become adult at 3 months of age and one female can produce 200 to 300 eggs per week. Embryos and larvae are transparent and develop outside of the mother, making the zebrafish a highly attractive model for developmental research. Most organs are developed at 72 hours post fertilization (hpf)[52]. The development of transgenic lines facilitated visualization of organ systems and physiological processes *in vivo* even further[53]. Zebrafish display a high degree of genetic, anatomical, and physiological similarities to humans[54]. Sequencing of the zebrafish genome revealed that around 70% of the zebrafish genes have a homologue in the human genome[55]. This has become of special interest with the development of targeted genome editing technologies such as the clustered regularly interspaced short palindromic repeats (CRISPR) system, which render the manipulation of specific genes possible[56].
The retinal anatomy and function have been highly conserved in vertebrates. The zebrafish retina as well as the mammalian retina consists of three nuclear layers and two plexiform layers. The cell bodies of cones and rods, the photoreceptors, are in the outer nuclear layer (ONL). In contrast to rodents, which are nocturnal animals and therefore have a rod dominated retina, zebrafish have a cone dominated retina, which is similar to the point of best visual acuity in the human retina, the fovea[57]. The cell bodies of retinal interneurons (horizontal, bipolar and amacrine cells) are in the inner nuclear layer (INL). The ganglion cell layer (GCL) contains the cell bodies of the ganglion cells (GC). The plexiform layers, which are found between the ONL and the INL as well as between the INL and the GCL, are the layers in which the retinal neurons interact via synapses. This structure can be found in both the zebrafish and the mammalian retina[58].
One key difference between the zebrafish and the mammalian retina is the origin and development of the retinal vasculature[59]. In mammals, the retinal vascular network, which consists of two vascular plexuses, undergoes intense remodelling during development. During early development, the hyaloid vasculature supplies the retina with blood flow. It regresses once the primary plexus begins growing into the retina. The switch in vessel origin happens at various time points, in humans it happens for example mid-gestation while in mice the switch happens at birth. During the development of the vasculature, the intraretinal vessels grow from the primary plexus via angiogenesis[60]. During the development of the zebrafish retinal vasculature, no switch in vessel origin occurs. The hyaloid vasculature develops in the first 5 days post fertilisation (dpf) and is at first tightly attached to the lens. It gradually loses contact with the lens and becomes attached to the retinal surface. Vessels do not grow into the retina[59]. However, most of the research concerning DR and utilizing zebrafish has been done on the vasculature, since zebrafish have distinct advantages including the availability of reporter lines, e.g. the *Tg(fli1a:EGFP)* line, and the early visualization in the larval retina[61].

Regulatory pathways of glucose homeostasis have been well conserved in zebrafish. Zebrafish larvae react to human insulin injection with inhibition of gluconeogenesis in the liver and hypoglycaemia and can develop insulin resistance[62]. Several isoforms of glucose transporters known in mammals have been found in zebrafish[63, 64]. Furthermore, zebrafish have a pancreas which is functionally very similar to humans. Both insulin-producing β-cells and glucagon-producing α-cells are present as early as 24hpf and their development is regulated through similar pathways to those in mammals[65]. These findings in combination with the possibility of targeted genetic manipulation explain the rising popularity of zebrafish in diabetes research[66].

1.6 The role of pancreatic duodenal homeobox factor-1 (pdx1) in diabetes

The gene pancreatic duodenal homeobox factor-1 (PDX-1) encodes a transcription factor that is essential for regulating pancreatic function and development. During development, PDX-1 is expressed in the whole pancreatic endoderm and crucial for the development of both exocrine and endocrine components of the pancreas. In the mature pancreas it is predominantly expressed in the insulin-producing β-cells[67]. It was shown that transfection of exogenous PDX-1 into pancreatic ductal epithelial cells, which, under normal circumstances, do not secrete insulin, *in vitro* stimulates the cells to express increased levels of PDX-1 and insulin mRNA and that the transfected cells respond to physiological stimuli such as elevated external glucose concentration[68].
PDX-1 is also known as insulin promotor factor-1 (IPF-1)[69]. In humans, it was found that a homozygous inactivating mutation in the coding sequence of IPF-1 leads to pancreatic agenesis and a heterozygous inactivating mutation is associated with maturity onset diabetes of the young type 4 (MODY4).[69, 70]
When comparing the alignment of the zebrafish protein with PDXs from other species it was shown that it had a high degree of similarity with other species including humans. Furthermore, in cross-sections of adult zebrafish tissue PDX-1 and insulin were expressed in the same regions located between the intestine and liver, which is where the zebrafish pancreas is located, leading to the conclusion that pdx1 structure, function and expression are highly conserved in zebrafish[71].
The analysis of the effects of the null mutation of *pdx1* in zebrafish (*pdx1*$^{-/-}$) indicated that a homozygous mutation leads to impaired pancreatic islet development and disrupted glucose homeostasis[72]. Subsequent analyses by the same group showed that these mutants exhibit distinct signs of retinal vasculature dysfunction, including vessel constriction, points of stenosis, a reduction of average vessel diameter, tortuous vessels with increased vessel density and increased sprouting and branching as well as a reduced expression of zonula occludens protein-1 (ZO-1). ZO-1 is a molecule that is integral to tight junctions which are responsible for connecting endothelial cells and regulating permeability in vessels. Furthermore, expression of GLUT1, the glucose transporter that is responsible for transport of glucose from the vasculature into the retinal tissue, was largely absent in mutants compared with wildtype controls[73]. Changes in GLUT1 expression have also been reported in DR patients and mouse models[74]. Parallel research on a CRISPR/Cas9-induced homozygous *pdx1*$^{-/-}$ mutant by our group independently observed the same findings of hypersprouting and hyperbranching in the adult zebrafish retina[31]. This study also described that a pharmacological modulation of VEGF and Nitric Oxide signalling rescues the hyperglycaemia-induced changes in the vasculature[31], further indicating that there are distinct similarities between the pathogenesis of DR in mammals and in zebrafish.

1.7 Aim of the thesis

Zebrafish have become an interesting model organism for diabetes and other metabolic disorders, especially due to the possibility of targeted genetic mutations[66]. The *pdx1*$^{-/-}$ zebrafish mutant has been studied by various groups in recent years, as the diabetic phenotype that can be produced in these mutants is very similar to that of other animal models of diabetes[72]. However, most of the studies concerning DR in zebrafish have been performed on vascular dysfunction and angiogenesis, as zebrafish are a highly suitable model for studying the vasculature due to the availability of various reporter lines[61].
The working hypothesis was that *pdx1*$^{+/-}$ zebrafish might have other pathologies associated with DR apart from angiogenesis. The aim of this thesis was the identification and establishment of protocols to analyse all components of the neurovascular unit in the zebrafish retina, as those might be of great benefit to all future research in the field.

2 MATERIAL AND METHODS

2.1 Material

2.1.1 Equipment

Product	Company
Agarose gel chamber	Peqlab Biotechnologie GmbH
Autostainer Link 48	Dako
BenchMark ULTRA IHC/ISH System	Roche
Benchtop centrifuge Rotina 420R	Hettich
BioPhotometer® D30	Eppendorf
Cell-F software	Olympus Opticals
Electrophoresis power supply	Consort
Gel Documentation Systems iX20 Imager	INTAS Science Imaging Instruments GmbH
Glucometer Freedom Lite	Abbott (FreeStyle)
Hamilton syringe (Glastight® #1705)	Hamilton
HistoCore Arcadia H Paraffin Dispenser for Histology	Leica
Leica TP1020 Automatic Benchtop Tissue Processor	Leica
Leica HI1210 Histology Water Bath for Paraffin Sections	Leica
Leica RM2165 Rotary Microtome	Leica
Leica TCS SP5 Confocal Microscope	Leica
Microcentrifuge Mikro 200R	Hettich
Microcuvette G1.0	Eppendorf
Olympus BX51 Microscope	Olympus
PCR cycler	BioRad
Table centrifuge	Carl Roth GmbH
U-HGLGPS Fluorescence Light Source	Olympus
XC10 camera	Olympus

2.1.2 Consumables

Product	Company
BD Microlance™ 3 (20G, 22G)	Becton, Dickinson and Company
Blood-glucose test stripes (Lite)	Abbot (FreeStyle Lite)
Biopsy processing/embedding cassettes with lid, green	neoLab
Conical tubes (15ml, 50ml)	Falcon
Cover slips (24x60mm)	Menzel-Gläser
Culture dishes (35x10mm, 60x15mm)	Thermo Fisher Scientific
Dumont Tweezers No. 5	neoLab
Feather disposable scalpel No. 10	Feather
Glass capillaries 1mm	World Precision Instruments
Microscope slides (76x26mm)	neoLab
Microscissors Vannas 2,5mm	Fine Science Tools
Microtome blades R35	Feather

Nitrile gloves	Semperguard
Pasteur pipettes	Brand GmbH & Co. KG
PCR tubes (0.2ml)	Star Labs
Petri dishes (10cm)	Greiner
Pipette filter tips (1000, 100, 20 and 10µl)	Nerbe plus GmbH
Pipette tip refills (1000, 200 and 10µl)	TipOne Star Labs
Pipettes (P1000, P200, P100, P20 and P2)	Gilson/Eppendorf
Safe-lock tubes (0.5, 1.5 and 2ml)	Eppendorf

2.1.3 Chemicals

All chemicals used during the experiments were purchased from the following companies (if not indicated separately):

Carl Roth GmbH & Co. KG
Merck AG
Roche Diagnostics GmbH
Sigma-Aldrich Chemie GmbH
Thermo Fisher Scientific Inc.

2.1.4 Buffers and Solution

2.1.4.1 Zebrafish maintenance and work

Buffer/solution	**Composition**
E3 (“eggwater”)	3g Red Sea Salt ad 10l MilliQ® water
0.1 M KCl	0.745g KCl ad 100ml MilliQ® water
1-phenyl-2-thiourea (PTU, 10x stock)	304mg PTU ad 1l MilliQ® water
Lysis buffer for genomic DNA	133µl of 1.5M Tris/HCl, pH8 40µl 0.5M EDTA 60µl Tween20 60µl Glycerol ad 20ml MilliQ® water
Tricaine (3-amino benzoic acidethylester)	400mg Tricaine powder 97.9ml MilliQ® water 2.1ml 1M Tris (pH 9) adjust to pH 7 100ml total volume
Tris/HCl, pH 7.8	181.17g Tris adjust pH to 7.8 with HCl ad 1l MilliQ® water
10x PBS	400g NaCl 10g KCl

	57.5g Na2HPO4 10g KH2PO4 ad 5l MilliQ® water
1x PBS	1l 10x PBS + 9l MilliQ® water
4% Paraformaldehyde (PFA)	4g PFA dissolved in 100ml 1x PBS
4% Formalin	100ml 37% formalin 100ml 10x PBS fill up to 1l with Aqua bidest

2.1.4.2 Gel electrophoresis

Buffer/solution	**Composition**
50x TAE buffer	232g Tris 57.1ml concentrated acetic acid 100ml 0.5 M EDTA, pH 8.6 ad 1l MilliQ® water
1x TAE buffer	100ml 50x TAE buffer ad 5l MilliQ® water

2.1.4.3 Digestion and staining procedures

Buffer/solution	**Compostion**
0.2M Tris-HCl, pH 7.45	24.22g Tris base 500ml Aqua bidest adjust pH to 7.45 with HCl fill up to 1L with Aqua bidest
3% Trypsin	1.5g trypsin 50ml 0.2M Tris-HCl
1% Periodic acid	2g periodic acid 20ml Aqua bidest fill up to 200ml with 96% ethanol
1x TBST	100ml 10x TBS stock solution 900ml Milli-Q® water 1ml Tween® 20 detergent
2% BSA	2g BSA in 100ml of 1x TBST

2.1.5 Kits and reagents

Product	**Company**
Aquatex® mounting medium	Millipore
Bluing Reagent	Ventana (Roche)
Dako REAL Target Retrieval Solution, pH6	Dako

Dako REAL Antibody Diluent	Dako
DPX mounting medium	Thermo Fisher Scientific
EnVision Flex DAB	Dako
Gene Ruler DNA ladder mix (0.5µg/µl)	Thermo Fisher Scientific
GoTaq® Green Master Mix	Promega
Haematoxylin II (modified after Mayer)	Ventana (Roche)
Mayer's hemalum solution	Millipore
OptiView DAB IHC Detection Kit	Ventana (Roche)
QIAquick PCR Purification Kit	QIAGEN
Schiff's fuchsine-sulfite reagent	Sigma-Aldrich
Shandon Cytology Formulation Consul-Mount	Thermo Fisher Scientific
Tricaine (3-amino benzoic acidethylester)	Sigma-Aldrich
Triton X-100 (1%)	Thermo Fisher Scientific
VectaShield HardSet mounting medium	Vector Laboratories
Ventana Cell Conditioner 2 (CC2)	Ventana (Roche)

2.1.6 Enzymes

Proteinase K was purchased from Roche.
Porcine Trypsin (1:250) was purchased from Sigma-Aldrich.

2.1.7 Oligonucleotides

Oligonucleotides were purchased from Sigma Aldrich (Merck KGaA).

2.1.7.1 Primer for genotyping (5'-3')

pdx1-genotyping-for	TTTCCCCGGTCTATGGCAAT
pdx1-genotyping-rew	TGGCCAAAGTACGAGTTACCT

2.1.8 Antibodies

2.1.8.1 Primary antibodies

Product	**Company**	**Dilution**
Mouse anti-GFAP	Millipore	1:4000
Rabbit anti-L-Plastin	GeneTex	1:500
Mouse anti-PCNA	Cell Signaling	1:2000
Rabbit anti-PDGFRβ	Cell Signaling	1:100
Rabbit anti-NG2 Chondroitin Sulfate Proteoglycane	Merck	1:200

2.1.8.2 Secondary antibodies

Product	**Company**	**Dilution**
Swine anti-rabbit TRITC	Dako	1:20
Chicken anti-rabbit Alexa Fluor 594	Thermo Fisher	1:100
OptiView HQ Universal Linker	Ventana (Roche)	1:20

2.1.8.3 Tertiary antibodies

Product	**Company**	**Dilution**
OptiView HRP Multimer	Ventana (Roche)	1:25

2.1.9 Zebrafish lines

Four transgenic zebrafish (Danio rerio) lines were used for all experiments: *wildtype (WT) Tg(fli1:EGFP)*[75], *WT Tg(nflk:EGFP)*[76], *pdx1*$^{+/-}$*/pdx1*$^{+/+}$ *Tg(fli1:EGFP)*[31] and *aldh2.1*$^{-/-}$ *Tg(fli1:EGFP)*[77].

2.2 Methods

2.2.1 Animal studies

2.2.1.1 Ethics

All experimental procedures on animals were approved by the local government authority Regierungspräsidium Karlsruhe (license number G-98/15) and by the Medical Faculty Mannheim (license number I-21/04) and carried out in accordance with the approved guidelines.

2.2.1.2 Zebrafish maintenance

Zebrafish embryos were raised in E3 medium ("eggwater") at 28.5°C with 0.003% 1-phenyl-2-thiourea (PTU) to suppress pigmentation. They were staged as described[52] and were referred to as larvae starting at 72h postfertilization (hpf). At 6 days postfertilization (dpf) the larvae were transferred to adult boxes and kept under a 13h light/11h dark cycle. At 90dpf, the zebrafish were referred to as adult. Adult zebrafish were fed daily with living shrimps *(Artemia salina)* in the morning and fish flake food in the afternoon.

2.2.1.3 Dissection of adult zebrafish

Adult zebrafish were taken from their tanks, transferred into single boxes and fasted overnight. In the morning they were fed with 0.5g flake food for 1h and then transferred to clean water for 1h of postprandial fasting. Afterwards, the fish were euthanized through hypothermal shock in 2-4°C cold water[78]. Blood for blood glucose measurement was collected from the caudal vein with a heparinized capillary as previously described[79]. The blood glucose measurement was performed using a glucometer. After the blood glucose measurement, zebrafish were beheaded and transferred into ice-cold PBS for dissection. For analyses of the retinae, the eyes were carefully extracted from the head using tweezers at the optic nerve and transferred into 4% PFA or 4% formalin for up to 48h. For confirmation of the genotype, the caudal fin was removed, transferred into 20µl of lysis buffer and processed further as described in chapter 2.2.4.

2.2.1.4 Microdissection of the retina for wholemount staining and digest preparation

Dissection of the retina was performed after an established protocol[80]. After removal from the fish head, the eye was transferred into a 1.5ml Eppendorf tube with 4% formalin and fixed for a different time depending on the intended following method (overnight at 4°C for wholemount staining/at least 48h at room temperature for digest preparation). After the fixation period, a petri dish was filled with 1x PBS and the eye was

carefully transferred into the petri dish. The eye was fixed with one tweezer at the optic nerve and the extraocular muscles as well as any residual extraocular tissue were removed with another tweezer. Still fixing the eye with one of the tweezers, the other scraped across the outer tissue of the eye consisting of the cornea and the sclera, also called the corneosclera, until the corneosclera could be removed entirely from the eye, leaving only the cup with the retina inside. The lens was carefully removed including all visible residues of the vitreous body. Before continuing with the next steps in the planned protocols, the retina was cut into a four-petal shape using microscissors.

2.2.1.5 Embedding for histology

After removal from the fish head, the eye was transferred into a 1.5ml Eppendorf tube with 4% formalin and fixed for at least 24h. For embedding in paraffin, after the fixation period the eye was placed inside an embedding cassette. Subsequently, the embedding cassette was placed inside the Leica TP1020 tissue processor for dehydration and infiltration with paraffin wax. After dehydration the cassettes were placed inside the paraffin tank of the HistoCore Arcadia H Embedding Station to avoid drying of the tissue. Using the heated forceps, the eye was removed from the cassette and placed carefully in an upright position with the optic nerve in a horizontal position inside a small mould. The mould was filled with paraffin and quickly moved to the cold spot to fixate the eye in the intended position. The mould was subsequently moved to the cooling plate until the paraffin was solid and the block could safely be removed from the mould. The paraffin block with the embedded eye was stored at -20°C until further usage.

2.2.1.6 Creating sections of paraffin embedded tissue

The paraffin block was taken straight from its storage at -20°C. A scalpel was used to cut the block into a square to create square sections. The block was subsequently fitted into the cassette clamp. A blade was put into the knife holder and fixed. The section thickness was set at 6µm. 6µm thick sections were cut off the block until the middle of the eye was cut, shortly before the optic nerve entered into the retina. To confirm the position, the sections were transferred into the water bath, which was set at 40°C, and mounted onto silanised microscope slides.
Shortly before the optic nerve was expected to enter into the retina, the section thickness was reduced to 3µm. From then on, 3µm thick sections were created for analysis of the neuroretina and for antibody staining. Only sections with optic nerve fibres were used in the experiments to ensure comparability and reproducibility.

2.2.2 Histology

2.2.2.1 Analysis of the neuroretina

To analyse the neuroretina for signs of degeneration, established protocols[81] were used with slight adjustments.

2.2.2.1.1 Periodic acid-Schiff's (PAS) stain

The 3µm thin sections were stained using the PAS stain. The PAS stain was performed by first deparaffinising the sections through putting them into an incubator at 37°C for 1h and leaving them to cool off for at least 15 minutes. Afterwards, they were put in two changes of xylene for 5 minutes each. The sections were subsequently rehydrated by placing them in ethanol with decreasing concentrations (99.9%, 96%, 80%, 70%)

for 5 minutes each and afterwards in aqua bidest. After having been washed in aqua bidest, the sections were placed in 1% periodic acid for 15 minutes and afterwards were washed briefly in aqua bidest again. They were placed in Schiff's fuchsine reagent for 15 minutes as well and were washed afterwards in lukewarm tap water for approximately two minutes until the sections turned pink. To counter-stain the nuclei the sections were placed in Mayer's hemalum solution for approximately two minutes and washed in lukewarm tap water again. Afterwards the sections were dehydrated by placing them in increasing concentrations of ethanol (70%, 80%, 96%, 99.9%) and two changes of xylene for 5 minutes each. After the last change of xylene cover slips were placed on top of the sections for microscopy using DPX mounting medium and left under the hood to dry.

2.2.2.1.2 Evaluation of the sections

The microscope slides with the stained sections were placed under a microscope and images were taken using the Cell-F software.

Of each section, four images were taken in both 200x and 400x magnification. Two images were taken to the left and to the right side of the optic nerve entrance into the retina and two images were taken in the peripheral parts of the retina at the transition to the cornea.

For the analysis of the retinal layer thickness, the images with 200x magnification were used. Using the tools in the Cell-F software, the thickness of every retinal layer was measured three times per image and the average of these three measurements was calculated for each layer. In zebrafish, the retina becomes significantly thinner in the periphery. Therefore, the central and the peripheral parts of the retina were evaluated separately.

For the analysis of the number of nuclei per layer, the images with 400x magnification were used. In analogy to how nuclei are counted in the rodent retina, nuclei in the ganglion cell layer (GCL) were counted over the whole length of the image, nuclei in the inner nuclear layer (INL) were counted over 150µm (3 x 50µm) and nuclei in the outer nuclear layer (ONL) were counted over 300µm (3 x 100µm). The average of each of the three cell counts per layer was calculated and the numbers in the central and the peripheral parts of the retina were evaluated separately.

2.2.2.2 Immunohistochemistry

All antibody stains on paraffin sections were established and performed in the Heidelberg Institute of Pathology using the BenchMark ULTRA IHC/ISH System or the Autostainer Link 48.

Wholemount antibody stains were performed manually according to established protocols.

2.2.2.2.1 PCNA and L-Plastin antibody staining procedure

The staining was done automatically by the BenchMark ULTRA IHC/ISH System after a specified protocol. Briefly, the paraffin sections were deparaffinised and preheated before adding Cell Conditioner 2 (CC2) to expose the antigen epitopes. The microscope slide was then heated to 90°C and incubated with CC2 for 40 minutes. In the next steps, the OptiView peroxidase inhibitor (3.0% hydrogen peroxide solution) was added first before adding the primary antibodies PCNA (1:2000) or L-Plastin (1:500), heating the slide to 36°C and incubating the slide with the primary antibody for 24

minutes. Afterwards the OptiView HQ Universal Linker was added. This mixture consisted of various secondary goat-anti-mouse and -anti-rabbit antibodies which bound to the primary antibodies. In the next step, the OptiView mouse tertiary antibody was added, which in turn was linked with horseradish peroxidase (HRP) and was made visible using a chromogen-substrate reaction, leaving a brown deposit. A counter stain was performed using Hematoxylin II and bluing reagent.

2.2.2.2.2 GFAP antibody staining procedure

The staining was performed using the Autostainer Link 48 after a specified protocol. Briefly, the slides were first deparaffinised and then the antigen epitopes were exposed through vapour pressure and the pH of the retrieval solution (in this case the retrieval solution had a pH of 6). To expose the antigen epitopes, the vapour pressure pot was filled with Aqua bidest until the floor of the pot was covered and a cuvette with Dako REAL Target Retrieval Solution was placed inside the pot. Both were heated to the point of boiling and then the microscope slides were placed inside the cuvette. The slides were boiled for 10 minutes and afterwards cooled down for 30 minutes inside the buffer solution. Afterwards the slides were incubated with first peroxidase inhibitor for 5 minutes, then the primary antibody (GFAP, 1:4000) for 30 minutes, FLEX/HRP for 20 minutes and FLEX DAB+ Sub-Chromo. Between each incubation, the slides were washed using fresh buffer solution. Counterstaining was performed using Mayer's hemalum solution for 1 minute and tap water for 10 minutes until the water turned blue. Cover slips were placed on top of the slides using Aquatex® or Consul-Mount mounting medium.

2.2.2.2.3 Analysis of PCNA and L-Plastin antibody stains

The analysis of PCNA and L-Plastin antibody stains was performed using light microscopy and the Cell-F software according to a published protocol[82]. Using a section in which the optic nerve enters into the retina, PCNA- or L-Plastin positive cells were counted over the length of the entire retinal section. The images used were taken at 200x magnification.

2.2.2.2.4 Analysis of GFAP antibody stains

The analysis of GFAP antibody stains was performed using light microscopy and the Cell-F software. Only sections on which the optic nerve enters the retina were used for the evaluation. Four images were taken at 400x magnification of each retinal section, one to the left and one to the right close to the optic nerve and one on each side in the periphery of the retina at the transition to the cornea. In each image, the number of GFAP positive cell processes was counted manually over 100µm. The number of GFAP positive cells was estimated by calculating the average of GFAP positive cells counted in the four images.

2.2.2.2.5 Wholemount retinal staining for NG2 and PDGFRβ

For wholemount retinal antibody staining, eyes were extracted from the fish head directly after decapitation and immersed in 4% formalin over night at 4°C. After fixation, the retina was dissected according to the established protocol[80]. Once the retina was dissected, it was washed in PBS three times for 30 minutes before being incubated at room temperature for one hour in permeabilization/blocking solution (1% BSA, 0.5% Triton-X100 in PBS). The primary antibody was then applied manually (rabbit anti-

NG2, 1:200 or rabbit anti-PDGFRβ, 1:100) and the retina was incubated with the primary antibody over night at 4°C. The next day, the retina was first washed shortly with PBS and then another three times for 30 minutes. After washing, the retina was incubated with the secondary antibody (either swine anti-rabbit TRITC, 1:20 in permeabilization/blocking solution for NG2 or chicken anti-rabbit Alexa Fluor 594, 1:100 in permeabilization/blocking solution for PDGFRβ) at room temperature for one hour. After adding the secondary antibody to the retina, the samples were kept in the dark to preserve the fluorescent signal. After incubation with the secondary antibody, the retina was washed again first shortly in PBS and then another three times for 30 minutes. After the last washing step, the retina was carefully transferred to a microscope slide with the inner part of the retina facing upwards. It was mounted with VectaShield Hard-Set mounting medium and directly visualized under the fluorescence lamp using the Cell-F software to take images.

2.2.3 Quantitative retinal morphometry

Quantitative retinal morphometry was performed based on an established protocol[83]. However, the method has not been used in zebrafish before. Therefore, it had to be adjusted for the use in zebrafish and validated before being used on the planned experimental groups.

2.2.3.1 Retinal digest preparation in zebrafish

After extracting the eye from the fish head, it was immersed in 4% formalin for fixation for at least 48h. After fixation, the retina was dissected after an established protocol[80]. After dissection, the retina was carefully placed inside a 35mm culture dish with aqua bidest using an aspirator and left in the incubator at 37°C overnight. The next morning, the retina was transferred into another culture dish filled with 3% trypsin and incubated again at 37°C for 1.5h. While the retina was incubated with trypsin, the needed instruments were prepared. An electric pump connected with an empty glass bottle for waste disposal on one side and infusion tubes with a 22G needle for aspiration on the other side was placed next to the stereomicroscope. A 5ml syringe was filled with aqua bidest, before placing a 25G needle on top of the syringe. Two barrier lines were applied on the microscope slides using the PAP pen to keep the water from running off the sides and to keep the digest preparation on top of the slide. After 1.5h, the culture dish was removed from the incubator and the retina was carefully placed on top of the microscope slide using an aspirator. The inner part of the retina was facing down and the retinal pigment epithelium (RPE) facing upwards. The vasculature was cleared from cells through dropping aqua bidest with the syringe on the retina. The residual cells were removed through water aspiration. This step was monitored under the microscope at the same time as the cells were removed to ensure that the vasculature was not aspirated as well. When the last of the cells were removed from the vasculature, the left-over aqua bidest was removed as far as possible through aspiration and the digests were left to air-dry.

2.2.3.2 Staining of endothelial cell (EC) and vascular mural cell (vMC) nuclei

To properly visualize the cell types in the retina, nuclei staining with undiluted Mayer's hemalum solution was performed. After air-drying the preparations, they were shortly placed in aqua bidest and then moved to fresh undiluted Mayer's hemalum solution for 7 minutes. Afterwards, they were placed in lukewarm tap-water for 2 minutes and then

moved shortly to 70% and then 80% ethanol before being put in first 96% and then 100% ethanol and kept there for 5 minutes each. After the last change of ethanol, the slides were placed in two changes of xylene and kept there for 5 minutes each as well, before the slides were covered with cover slips and using DPX mounting medium.

2.2.3.3 Analysis of the vasculature in wildtype zebrafish

To determine the average number of ECs and vMCs in the zebrafish retina, six retinae of transgenic *Tg(nflk:GFP)* were used.

2.2.3.3.1 Identification of endothelial cells

In transgenic *Tg(nflk:GFP)* zebrafish, the nuclei of endothelial cells express green fluorescent protein (GFP). After digestion and before nuclei staining, images of the retinal digest preparations were captured using a confocal microscope (Leica TCS SP5). Images were taken with 600Hz, 1024 x 1024 pixels. After capturing the images, the digest preparations were stained according to step 2.2.3.2. and images of the same areas were captured using light microscopy. The images of corresponding areas were compared to identify the nuclei that correspond to endothelial cells.

2.2.3.3.2 Counting of ECs and vMCs in wildtype retinae

After determining the shape and position of ECs and vMCs in the vasculature, images were taken in the different areas of the retina, since whole retinae can be divided into three different areas according to their vessel density: low (25%), middle (50%) and high density (25%). In each area, six different images were taken of the digest preparation. One image was taken where the optic artery splits into the 5-7 main vessels[80] of the zebrafish retina. Two images were taken in the middle part of the retina in each area and three images were taken in the peripheral part of the retina, where the vessels connect to the inner optic circle (IOC).
In each of the images, ECs and vMCs were counted manually using the Cell-F software on vessels that could be visualized in a straight line for 200µm to ensure comparability.

2.2.3.4 Protocol for quantitative retinal morphometry in zebrafish

To ensure comparability and reproducibility, images that are evaluated in experimental groups need to come from the same part of the retina (central, middle or peripheral). As the best results can be produced from vessels in the middle part of the retina, these images were used going forward. After preparing the retinal digest and staining the nuclei, eight images of the middle part of the retina were taken in each retina. In these images, the ECs and vMCs were counted manually using the Cell-F software in vessels that could be visualized over 200µm. To achieve comparability with the evaluation of rodent retinal digest preparations, in which ECs and vMCs are counted as cells/mm^2 capillary area, the diameters of the vessels were measured as well. With these data, numbers of ECs and vMCs were calculated per mm^2 capillary area.

2.2.4 Molecular biology

The induction of the *pdx1*$^{+/-}$ mutated zebrafish line was performed using the CRISPR/Cas9 method[31]. Zebrafish with a frame-shift mutation close to the target sequence were used to establish a stable F2 generation. To prove the genotype in the

zebrafish used in experiments, genomic DNA was isolated and analysed using polymerase chain reaction (PCR).

2.2.4.1 Isolation of genomic DNA

Genomic DNA was obtained from the caudal fin of the zebrafish. After either anaesthesia using tricaine or euthanasia using hypothermal shock the tip of the caudal fin was removed and placed in 20µl of lysis buffer inside a 0.2ml Eppendorf tube. The following steps were programmed in the thermocycler:

- 98°C 10min
- add 10µl of proteinase K
- 55°C at least 4h/over night

- shake the tube to dissolve the fin
- 55°C 1h
- 98°C 10min
- hold at 8°C

2.2.4.2 Polymerase chain reaction (PCR)

Primers (2.1.7.) were used to multiply the DNA strains.

PCR mix
- 1.5µl forward primer and 1.5µl reverse primer
- 12.5µl GOTaq® green master mix
- 7.5µl autoclaved H_2O
- 2µl genomic DNA

PCR program thermocycler
- 95°C 3min

- 95°C 30s
- 55°C 30s
- 72°C 45s
- repeat 35x

- 72°C 10min
- hold at 4°C

2.2.4.3 Gel electrophoresis

A 2% agarose gel was created using 2g of agarose, 100ml of 0.5x TAE buffer and 10µl of ethidium bromide. 2µl of PCR product were placed in the gel pockets and divided in 0.5x TAE at 120V and 150W for 45 minutes.

2.2.4.4 Purification and sequencing of the PCR product

The QIAquick PCR purification kit was used according to the manufacturer's protocol to purify the PCR product. DNA extraction was performed using autoclaved H_2O and afterwards the DNA-concentration was analysed photometrically (λ = 260nm; λ =

280nm). To sequence the DNA, the “TubeSeq Service” at eurofinsgenomics.eu was used. Analysis of the gene sequence was performed using Poly Peak Parser[84].

2.2.5 Imaging

Images of paraffin sections were taken using the BX51 upright microscope (Olympus Life Science) with the XC10 camera (Olympus Life Science). Images of wholemount antibody stains were taken using the BX51 upright microscope with the Olympus U-HGLGPS fluorescence light source (Olympus Life Science) and the XC10 camera (Olympus Life Science). Images of the *Tg(flk:GFP)* zebrafish retinae were taken using a DM6000 B confocal microscope with a Leica TCS SP5 DS system.

2.2.6 Software

Analysis of paraffin sections, wholemount antibody stains and digest preparations was performed using the Cell-F software (Olympus Opticals). Confocal visualization of the retinal vessels was performed using the LAS AF Lite Software (Leica). Statistical analyses were performed using GraphPad Prism 6.01 and 8.3.0.

2.2.7 Statistical analysis

All results are presented as mean with standard deviation (mean ± SD). To analyse the statistical significance between different groups, Student’s unpaired t-test or one-way ANOVA (followed by either Sidak’s or Tukey’s post-hoc multiple comparisons test) were performed in GraphPad Prism 6.01 or 8.3.0. A p-value of 0.05 was considered as significant: *$p<0.05$, **$p<0.01$, ***$p<0.001$, ****$p<0.0001$.

3 RESULTS

3.1 Analysis of neurodegeneration

3.1.1 Adaptation of the rodent neurodegeneration protocol in zebrafish

One of the main pathologies associated with DM is retinal neurodegeneration. This can be observed morphologically as ganglion cell (GC) loss, apoptosis of amacrine cells in the inner and outer nuclear layer as well as photoreceptors, which leads to the thinning of the retinal layers. We therefore needed to analyse the utilization protocol used for the study of neurodegeneration in the mammalian retina in the zebrafish retina. There was one notable difference when comparing rodent and zebrafish retinae: In zebrafish, the ONL was thinner than the INL while in rodents the INL was thinner than the ONL. Apart from this observation, the protocol could be used in zebrafish without any adaptations (Fig. 1).

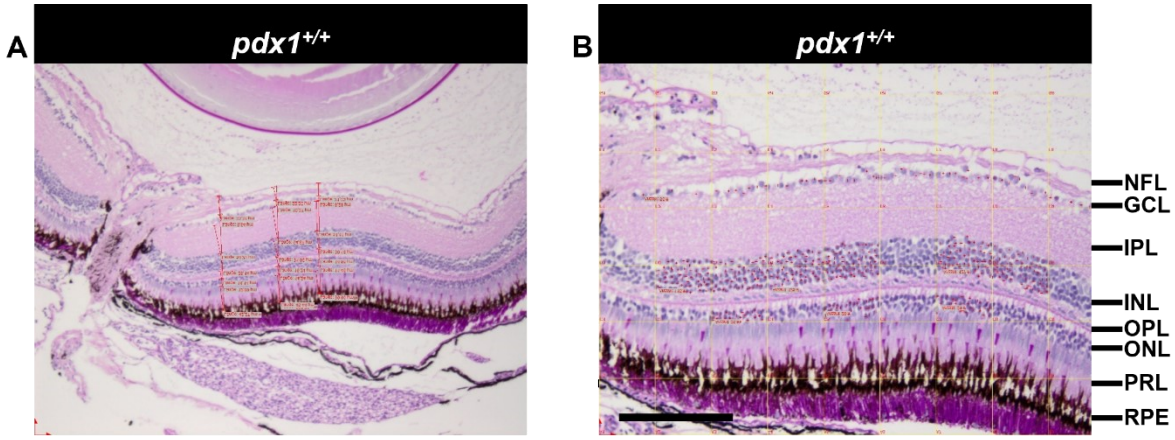

Figure 1: Analysis of neurodegeneration in zebrafish. Paraffin sections (3µm) were analysed with light microscopy after PAS staining. A) 100x magnification of the zebrafish retina. The red lines mark where retinal layer thickness was measured. B) 200x magnification of the zebrafish retina with explanation of the different layers. The yellow squares have a side length of 50µm each. The red crosses indicate the counted cell nuclei. Scale bar: 100µm. Abbreviations: NFL = nerve fibre layer, GCL = ganglion cell layer, OPL = outer plexiform layer, ONL = outer nuclear layer, IPL = inner plexiform layer, INL = inner nuclear layer, PRL = photoreceptor layer, RPE = retinal pigment epithelium.

3.1.2 Experimental setting

There are various factors still unknown about the zebrafish retina. One specific factor which is important to consider when studying the zebrafish retina is that in contrast to the mammalian retina the zebrafish retina can regenerate. As this may disrupt the results in the analysis of retinal neurodegeneration, we were interested to see whether there are any differences in retinal layer thickness between different zebrafish lines.
A comparison of the retinae of transgenic *wildtype (WT) Tg(fli1:EGFP)* zebrafish to those of both *pdx1*$^{+/-}$ *Tg(fli1:EGFP)* and *pdx1*$^{+/+}$ *Tg(fli1:EGFP)* at 20 mpf found that the total retinae of the fish from the WT line were thinner than those from the *pdx1* line ($p < 0.0001$). There was a change in individual layers as well. Both in close proximity to the optic nerve and in the periphery of the retina the IPL was thinner in *WT Tg(fli1:EGFP)* zebrafish than in fish from the *pdx1 Tg(fli1:EGFP)* line and in the periphery the PRL was significantly thinner in *WT Tg(fli1:EGFP)* zebrafish than in *pdx1*$^{+/-}$

Tg(fli1:EGFP) zebrafish. There was no considerable difference in any retinal layer between *pdx1*$^{+/+}$ and *pdx1*$^{+/-}$ zebrafish. This led to the conclusion, that comparisons between different experimental groups should always be analysed between fish from the same genetic line ("littermates"), since there are considerable differences between different zebrafish lines (Fig. 2).

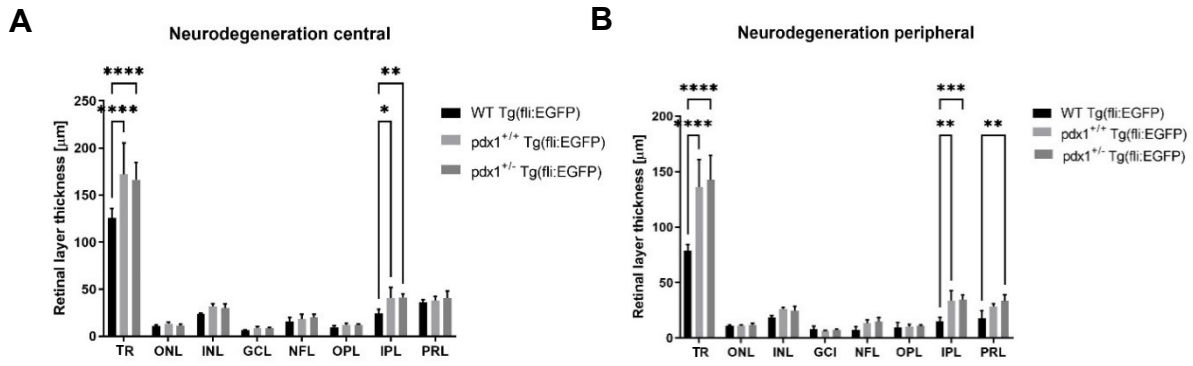

Figure 2: Transgenic *WT Tg(fli:EGFP)* zebrafish have thinner retinae than zebrafish from the *pdx1 Tg(fli:EGFP)* line. A) Retinal layer thickness in the central retina. B) Retinal layer thickness in the peripheral retina. Abbreviations: TR = total retina, ONL = outer nuclear layer, INL = inner nuclear layer, GCL = ganglion cell layer, NFL = nerve fibre layer, OPL = outer plexiform layer, IPL = inner plexiform layer, PRL = photoreceptor layer.

3.1.3 *pdx1*$^{+/-}$ zebrafish do not show consistent signs of neurodegeneration throughout their lifecycle

To establish whether neurodegeneration is present at any time point around the beginning of retinal angiogenesis in *pdx1*$^{+/-}$ zebrafish, a comparison of retinal layer thickness and neuronal nuclei numbers at different time points was performed on zebrafish at 12 mpf and 21 mpf. The onset of postprandial hyperglycaemia in *pdx1*$^{+/-}$ zebrafish has been shown to occur at 18 mpf[31]. Blood glucose was measured in all compared experimental groups, however, the zebrafish analysed in these experiments did not suffer from measurable postprandial hyperglycaemia (Fig. 3).

At 12 mpf, a relevant difference was detectable close to the optic nerve when measuring the total retinal thickness but could not be traced back to any specific layer. *Pdx1*$^{+/+}$ zebrafish had a total retinal thickness of 189.30 ± 20.07µm while *pdx1*$^{+/-}$ zebrafish had a total retinal thickness of 173.23 ± 25.71µm (mean ± standard deviation (SD), $p < 0.05$). In the periphery there was no significant change in any retinal layer.

At 21 mpf, there was no significant change in any layer or the total retina when comparing *pdx1*$^{+/-}$ zebrafish and their littermates, indicating that compensation of the phenotype took place between the two time points. The only visible tendency was that in the peripheral parts of the retina, the retinae of *pdx1*$^{+/-}$ mutants were thicker than the retinae of their littermates, however, this change was not statistically significant (Fig. 4).

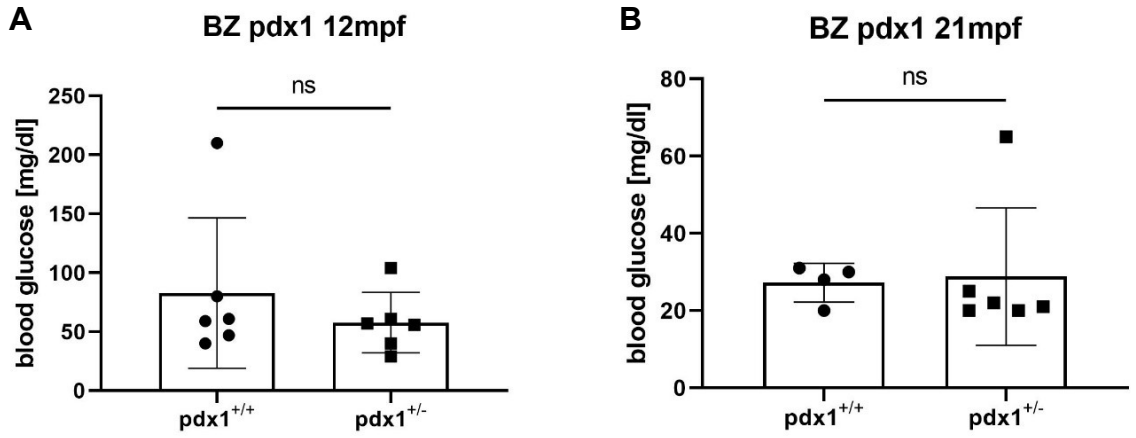

Figure 3: No observable increase in postprandial blood glucose [mg/dl] in *pdx1*$^{+/-}$ zebrafish. A) Comparison of postprandial blood glucose at 12 mpf (*pdx1*$^{+/+}$ n=6, *pdx1*$^{+/-}$ n=6). B) Comparison of postprandial blood glucose at 21 mpf (*pdx1*$^{+/+}$ n=4, *pdx1*$^{+/-}$ n=6).

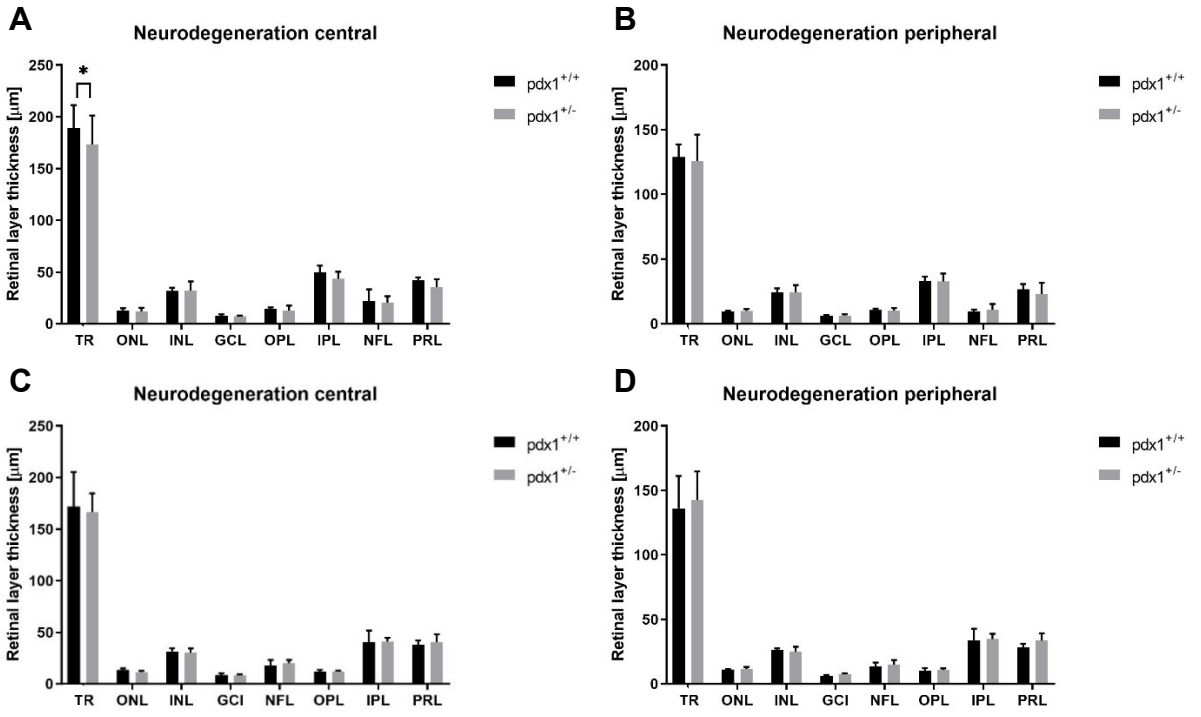

Figure 4: *pdx1*$^{+/-}$ mutants do not show consistent signs of neurodegeneration throughout their lifecycle. A and B) Retinal layer thickness in *pdx1*$^{+/-}$ zebrafish (n=6) and their littermates (n=5) at 12 mpf. C and D) Retinal layer thickness in *pdx1*$^{+/-}$ zebrafish (n=6) and their littermates (n=4) at 21 mpf.

Neuronal nuclei numbers were not reduced at any stage (supplementary material), indicating no loss of GCs, which is considered a typical sign of neurodegeneration in rodent models of DR and in human diabetic patients.

All the above indicates that there were no consistent signs of neurodegeneration at any point in the lifecycle of *pdx1*$^{+/-}$ zebrafish. Furthermore, observable differences at one point during the experiment did not persist. The reason for this is most likely that the zebrafish retina can regenerate. This makes it difficult to analyse the zebrafish retina for signs of neurodegeneration, as constant regeneration may mask degenerative processes.

3.1.4 Increased nuclei in the INL in *pdx1*$^{+/+}$ zebrafish at 12mpf

The analysis of retinal layer thickness revealed that there was no reproducible change between *pdx1*$^{+/-}$ zebrafish and their littermates. However, at certain time points there were observable and statistically significant changes in the total retinal layer thickness which indicated that some form of permanent disruption was happening in the retinae of *pdx1* zebrafish.

Zebrafish embryos develop outside of the mother and start feeding independently at 5 days post fertilization (dpf). Before that they rely on the yolk sack as an energy source for development. It has been shown that the yolk is metabolically active and processes lipids before they are mobilized into the embryonic body[85]. As all lipids and enzymes that are present in the yolk come from the mother animal and the mother animals of *pdx1*$^{+/+}$ zebrafish are themselves *pdx1*$^{+/-}$ zebrafish with an impaired glucose homeostasis, we hypothesised that potential changes in retinal layer thickness may become distinguishable by introducing a second *pdx1*$^{+/+}$ zebrafish line (*pdx1*$^{+/+}$ F2) which descends from *pdx1*$^{+/+}$ parents instead.

A comparison of retinal layer thickness and the numbers of neuronal nuclei at 4 mpf (zebrafish are considered adult at 3 mpf) and 12 mpf (Fig. 5) was therefore performed. At 4 mpf, *pdx1*$^{+/-}$ zebrafish showed a significantly thinner total retina in comparison with *pdx1*$^{+/+}$ zebrafish (central: *pdx1*$^{+/+}$ 164.12 ± 7.01 µm vs. *pdx1*$^{+/-}$ 149.46 ± 4.42 µm, $p < 0.0001$, peripheral: *pdx1*$^{+/+}$ 119.23 ± 7.62 µm vs. *pdx1*$^{+/-}$ 93.65 ± 4.75 µm, $p < 0.0001$) even though the effect could not be traced back to one specific layer. Only in the peripheral parts of the retina, the PRL was significantly thinner in *pdx1*$^{+/-}$ zebrafish than in *pdx1*$^{+/+}$ zebrafish (*pdx1*$^{+/+}$ 21.02 ± 3.18 µm vs. *pdx1*$^{+/-}$ 12.71 ± 2.18 µm, $p < 0.01$), indicating less developed or fewer photoreceptors. At 12 mpf there was no significant change in retinal layer thickness, again indicating a compensation of the phenotype through regeneration. However, at this point, an increase in neuronal nuclei in the INL in the periphery of the retina of this new line of *pdx1*$^{+/+}$ zebrafish could be observed in comparison to *pdx1*$^{+/-}$ zebrafish (*pdx1*$^{+/+}$ 120.83 ± 15.33 nuclei/100µm vs. *pdx1*$^{+/-}$ 101.03 ± 18.69 nuclei/100µm, $p < 0.05$). This further indicated that it is possible that the retinae of *pdx1*$^{+/-}$ zebrafish sustained damage which needed to be regenerated (increased number of nuclei due to cell division) but could not be quantified through measurement of retinal layer thickness.

3.1.5 *pdx1*$^{-/-}$ zebrafish do not show signs of neurodegeneration

Due to the low survival of *pdx1*$^{-/-}$ mutants, only a few eyes that were already embedded in paraffin could be analysed over the course of these experiments. Paraffin slides of 18 month old CRISPR/Cas9 induced *pdx1*$^{-/-}$ mutants did not show thinning of retinal layers or decreased numbers of neuronal nuclei (supplementary material). However, this fish population does show significant angiogenesis at the same time point[31], indicating more clearly that in zebrafish neurodegeneration most likely does not precede microvasculopathy or at least that the process of retinal regeneration makes it difficult to conclusively prove that neurodegeneration is taking place in the zebrafish retina.

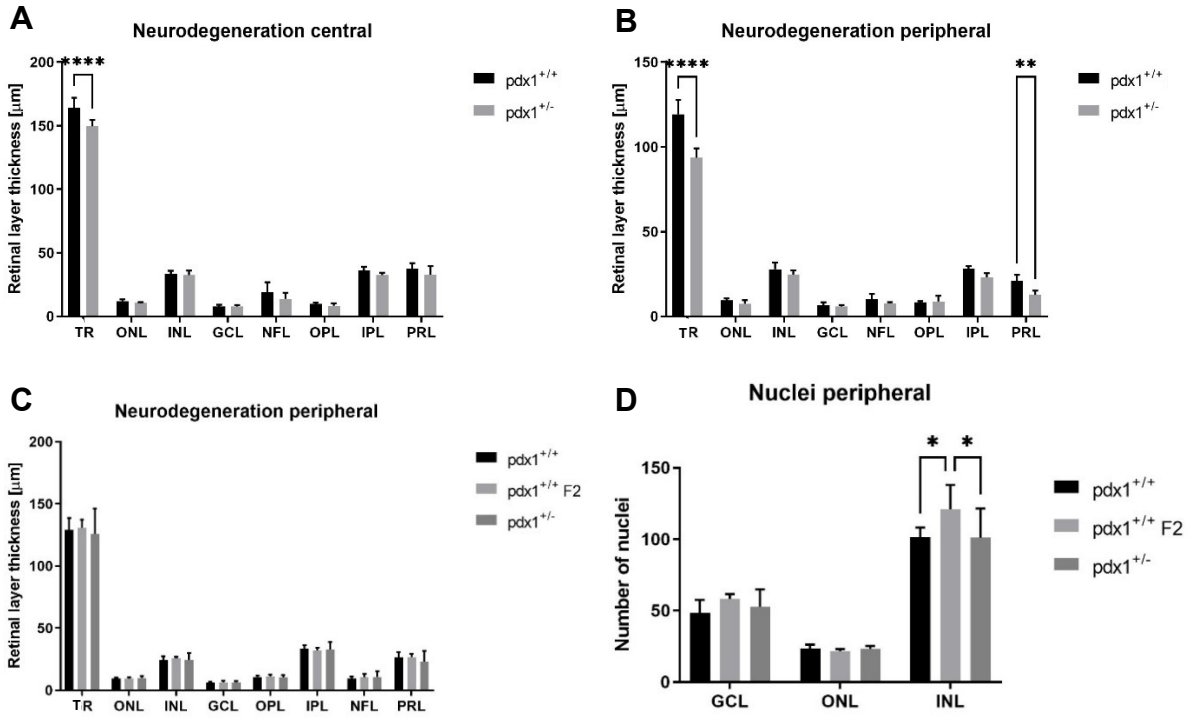

Figure 5: *pdx1*$^{+/-}$ zebrafish exhibit decreased retinal thickness at 4mpf and fewer neuronal nuclei in the INL in the periphery of the retina at 12mpf. A and B) Retinal layer thickness in *pdx1*$^{+/-}$ zebrafish (n=6) and *pdx1*$^{+/+}$ zebrafish (n=6) at 4 mpf. C) Peripheral retinal layer thickness in *pdx1*$^{+/-}$ zebrafish (n=6), their *pdx1*$^{+/+}$ littermates (n=5) and *pdx1*$^{+/+}$ zebrafish (n=6) at 12 mpf. D) Number of neuronal nuclei in *pdx1*$^{+/-}$ zebrafish (n=6), their *pdx1*$^{+/+}$ littermates (n=5) and *pdx1*$^{+/+}$ zebrafish (n=6) at 12 mpf.

3.2 Analysis of proliferation in the zebrafish retina

3.2.1 Proliferation is not significantly increased in *pdx1*$^{+/-}$ mutants

To address whether there was increased proliferation as an indication for an increased need for regeneration in *pdx1*$^{+/-}$ zebrafish, we stained paraffin sections of the zebrafish retina with an anti-PCNA (proliferating cell nuclear antigen) antibody. PCNA is expressed on proliferating cells and is regularly used as a proliferation marker in the zebrafish retina.

PCNA positive cells were visible in paraffin sections of wildtype and of mutant zebrafish (Fig. 6), indicating that proliferation was happening in all zebrafish retinae, consistent with the hypothesis that zebrafish retinae constantly regenerate.

The PCNA positive cells were mostly localized in either the ONL or the GCL, indicating that photoreceptors and ganglion cells are the cells that typically need regeneration in the *pdx1* zebrafish line.
There was no increase in PCNA-positive cells between *pdx1*$^{+/-}$ zebrafish and *pdx1*$^{+/+}$ zebrafish at 12 mpf (Fig. 7). On average, there were between 10.5 ± 1.93 PCNA positive cells in the *pdx1*$^{+/-}$ retina and 11.6 ± 2.79 PCNA positive cells in the *pdx1*$^{+/+}$ retina. All the above indicates that proliferation is not increased in the *pdx1*$^{+/-}$ mutants.

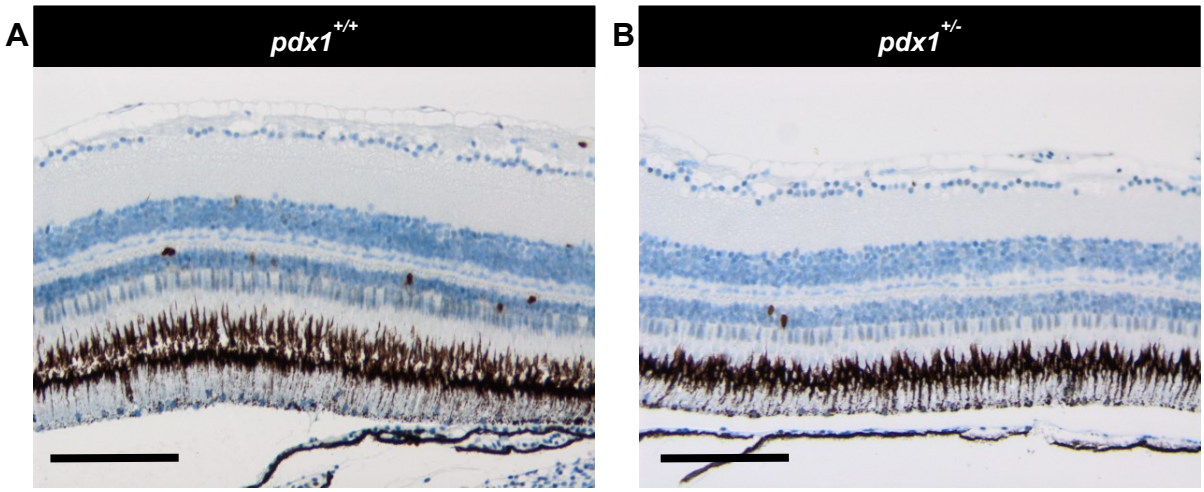

Figure 6: PCNA as a proliferation marker in the zebrafish retina. A) 200x magnification of a *pdx1*$^{+/+}$ retina. B) 200x magnification of a *pdx1*$^{+/-}$ retina. Anti-PCNA antibody, DAB stain. Nuclei counter stained with haematoxylin and bluing agent. Scale bar: 100µm.

3.2.2 Increased number of PCNA positive cells in *pdx1*$^{-/-}$ mutants at 18mpf

In 18 mpf *pdx1*$^{-/-}$ mutants there was an increase of PCNA positive cells (Fig. 7). The littermates at the same age had on average 15.6 ± 3.34 PCNA positive cells per retinal section, the mutants had on average 53.6 ± 19.31 PCNA positive cells. However, this difference was not statistically significant since only two of the *pdx1*$^{-/-}$ mutants had very high numbers of PCNA positive cells, while the other were comparable to their littermates. This indicates a potential cluster building process with high- and low-proliferating specimen. However, due to the low survival of the *pdx1*$^{-/-}$ mutants, this hypothesis could not be further verified.

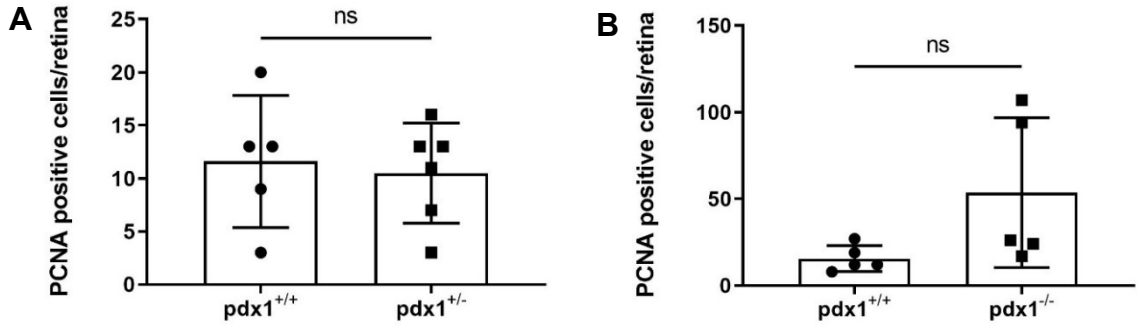

Figure 7: No increased proliferation in *pdx1* zebrafish. A) No signs of increased proliferation in *pdx1*$^{+/-}$ zebrafish. *pdx1*$^{+/-}$ (n=6), *pdx1*$^{+/+}$ (n=5) B) Potential cluster of high-proliferating specimen in the *pdx1*$^{-/-}$ group. *pdx1*$^{-/-}$ (n=5), *pdx1*$^{+/+}$ (n=5).

3.3 Analysis of reactive gliosis

3.3.1 Similar GFAP expression in both *pdx1*$^{-/-}$ and *pdx1*$^{+/-}$ mutants and their corresponding littermates

Müller glial cells are the resident macroglia and the main glial cell type of the retina. Under hyperglycaemic conditions Müller cells of the mammalian retina become activated ("reactive gliosis"). The most common marker of reactive gliosis is the upregulation of glial fibrillary acidic protein (GFAP). In zebrafish, Müller cells are the main driver of retinal regeneration.

To visualize Müller cell activation in zebrafish, we stained paraffin sections of the retina with an anti-GFAP antibody. While in rodent models Müller cells in control retinae do not express GFAP, we found that Müller cells in the retinae of both littermates and mutant zebrafish express GFAP (Fig. 8). There were also no evident signs of morphological changes of the Müller glial cells in the *pdx1* mutants.

There was overall no discernible change in the number of GFAP positive cells between *pdx1*$^{+/-}$ or *pdx1*$^{-/-}$ and their corresponding littermates. Yet, there was an increased number of GFAP positive cells in the retinae of the *pdx1*$^{+/+}$ line that descends from two *pdx1*$^{+/+}$ parents (*pdx1*$^{+/+}$ 12.33 ± 0.32 GFAP positive cells/100µm, *pdx1*$^{+/-}$ 10.83 ± 0.27 GFAP positive cells/100µm, $p < 0.01$). This is consistent with the finding that the same fish had an increased number of neuronal nuclei in the INL. An increased activation of Müller glia cells could be indicative of increased proliferation which would explain the elevated cell numbers.

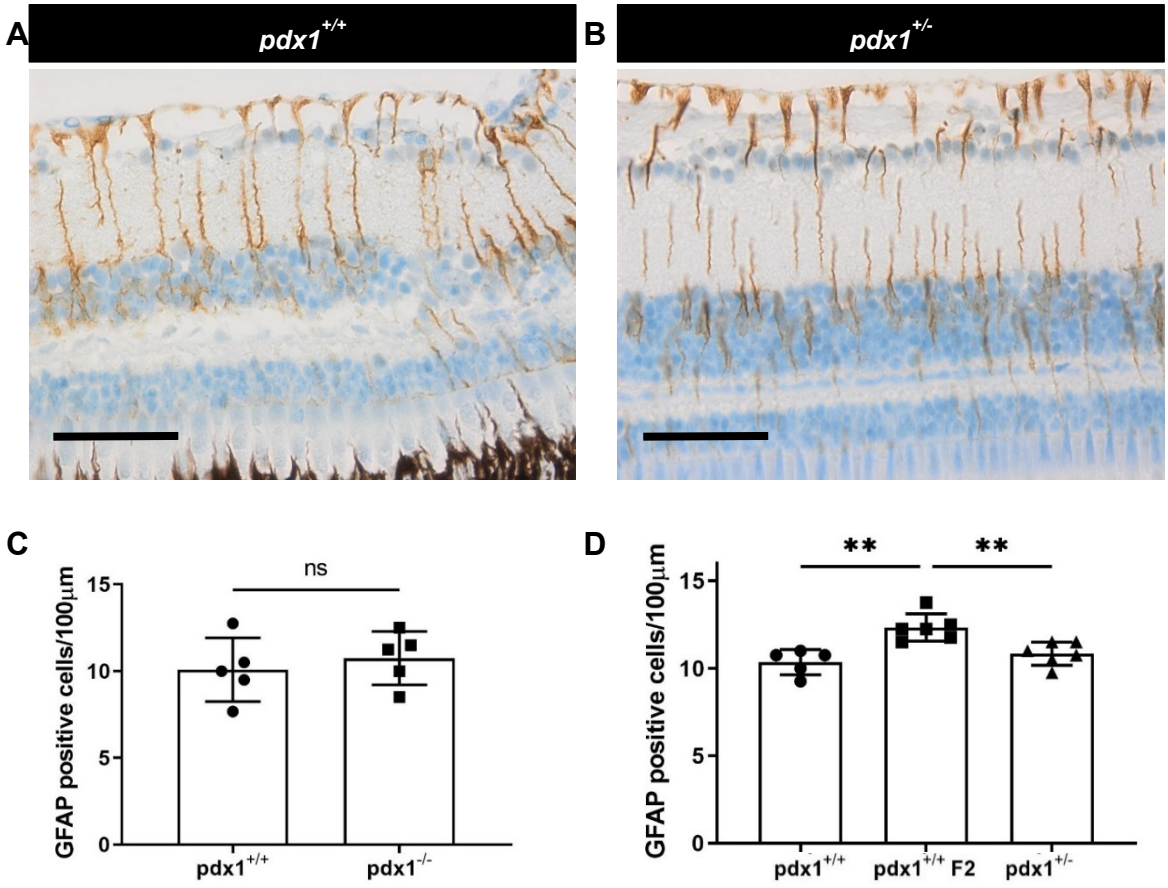

Figure 8: No significant change in GFAP positive cells/100µm in pdx1$^{-/-}$ and pdx1$^{+/-}$ zebrafish in comparison to their littermates. A) 400x magnification of a pdx1$^{+/+}$ retina. B) 400x magnification of a pdx1$^{+/-}$ retina. A and B) Anti-GFAP antibody, DAB stain. Nuclei counter stained with haematoxylin and bluing agent. Scale bar: 100µm. C) Comparison of GFAP positive cells/100µm between pdx1$^{-/-}$ mutants (n=5) and their littermates (n=5). D) Comparison of GFAP positive cells/100µm between pdx1$^{+/-}$ mutants (n=6), their littermates (n=5) and pdx1$^{+/+}$ F2 zebrafish (n=6).

3.4 Analysis of microglia activation

3.4.1 *pdx1*$^{-/-}$ and *pdx1*$^{+/-}$ mutants do not exhibit increased microglia activation in comparison to their corresponding littermates

Microglia represent the resident macrophage population in the retina and the central nervous system. Under physiological conditions they help to maintain retinal integrity, while under pathological conditions they can trigger auto-destructive responses.
L-Plastin is a specific marker of leukocytes, including macrophages, in zebrafish. As microglia are the resident macrophages of the retina, L-Plastin can be used to mark microglia in retinal paraffin sections. L-Plastin positive cells were easily distinguishable on retinal paraffin sections and could be quantified like PCNA positive cells over whole sections of the retina (Fig. 9). Most of the L-Plastin positive cells were localized at the borders of the plexiform layers. This is as expected from other species such as rats or mice. Overall, there was no observable increase in microglia numbers between the *pdx1*$^{-/-}$ or *pdx1*$^{+/-}$ mutants and their respective littermates.

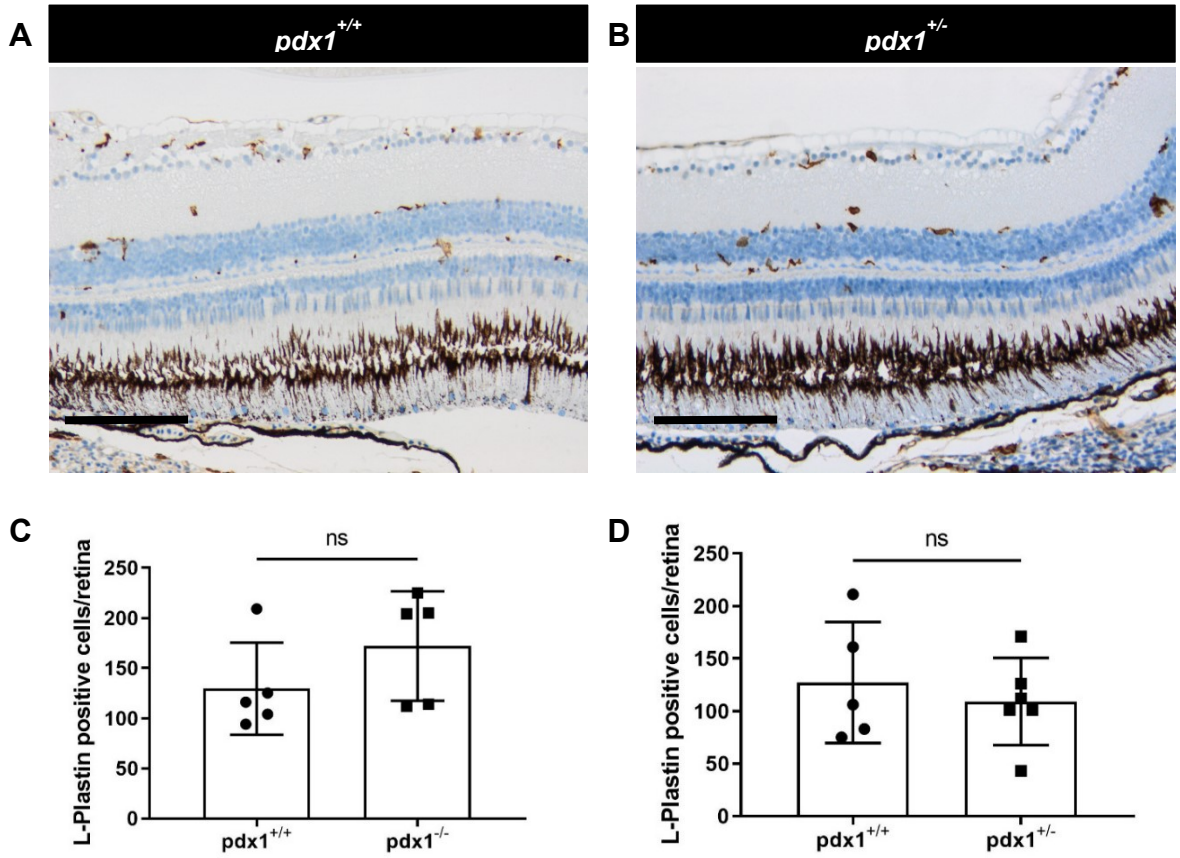

Figure 9: No significant change between *pdx1*$^{-/-}$ or *pdx1*$^{+/-}$ mutants and their corresponding littermates. A) 200x magnification of a *pdx1*$^{+/+}$ retina. B) 200x magnification of a *pdx1*$^{+/-}$ retina. A and B) Anti-L-Plastin antibody, DAB stain. Scale bar: 100µm. C) No significant difference between *pdx1*$^{-/-}$ zebrafish and their littermates. D) No significant difference between *pdx1*$^{+/-}$ mutants and their littermates.

3.4.2 Evidence of cluster formation regardless of the experimental group

Regardless of the experimental group, there were sections with a visible cluster formation of L-Plastin positive cells with no histologically obvious evidence of retinal damage (Fig. 10). The fact that the zebrafish retina is capable of regeneration is compatible with the observation that microglia infiltrate the retina when any form of damage is detected and that this damage does not necessarily have anything to do with the genotype or other factors of the specific zebrafish's environment.
This observation further establishes that the L-Plastin stain is a viable method for detecting increased microglial activation.

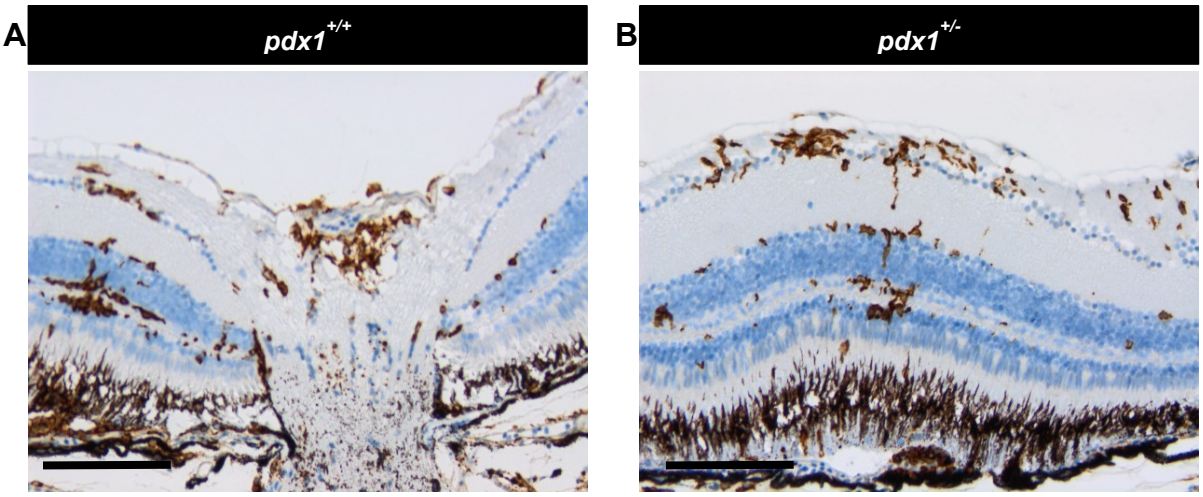

Figure 10: Evidence of cluster formation regardless of experimental group. A) Cluster formation of L-plastin positive cells in the GCL, around the OPL and at the optic nerve entrance into the retina of a *pdx1*$^{+/+}$ F2 littermates. B) Cluster formation of L-plastin positive cells in the GCL/NFL and around the OPL of a *pdx1*$^{+/-}$ zebrafish. A and B) 200x magnification. Anti-L-Plastin antibody, DAB stain. Scale bar: 100µm.

3.5 Quantitative retinal morphometry

3.5.1 The zebrafish retinal digest preparation

A critical feature of DR is microvascular dysfunction, which is associated with increased vascular permeability because of endothelial dysfunction and loss of pericytes. The most commonly used protocol to analyse the loss of endothelial cells and pericytes is the retinal trypsin digest protocol[83]. During the work on this thesis, this protocol was performed for the first time on the zebrafish retina.

One main difference between a retinal trypsin digest of the mammalian retina and of the zebrafish retina is that while mammals have different vascular plexus that supply the retina with nutrients, zebrafish only have one on top of the retina[59]. The zebrafish retinal vasculature is well structured[80]. At the entrance into the retina, the optic artery splits into on average 5-7 main vessels which in turn split up on average two more times before connecting in the periphery to form the circumferential vein, also known as the inner optic circle (IOC). This structure was also visible after performing the digest protocol on the zebrafish retina.

Three different cell types were visible after staining the digest preparation with Mayer's hemalum solution (Fig. 11). Inside the vessel wall there were oval nuclei which took on a light purple colour. On top of the vessels with some distance between the nuclei and the vessel wall were long and flat nuclei which took on a dark purple colour. Furthermore, there were small and round nuclei which took on a very dark colour and could be found both inside and around the vessels. Those were most likely erythrocytes, as zebrafish erythrocytes possess nuclei[86]. It has been shown before that both endothelial cells and pericytes are present in the zebrafish retinal vasculature via electron microscopy[59] and antibody staining[87]. However, as the zebrafish vasculature has not been subjected to quantitative retinal morphometry using trypsin digests, a novel protocol to distinguish endothelial cells from pericytes had to be established.

The transgenic *Tg(flk:GFP)* line was utilized to identify endothelial cells in retinal digest preparations. Identification of features (Fig. 12) made it possible to be confident that the vessels that were compared were indeed the same vessels.

The combination of GFP expression flat mounts and vascular cell annotation yielded that endothelial cells were the oval-shaped, moderately HE positive cells that were located within the vessel.

To confirm the position of pericytes on top of the vessels we used NG2 and PDGFRβ antibody stains on retinal wholemounts. Putative pericytes were positive, those were however situated mainly on the IOC (Fig. 13). As this made it impossible to clearly identify the mural cells as pericytes, we called those cells mural cells from that point on.

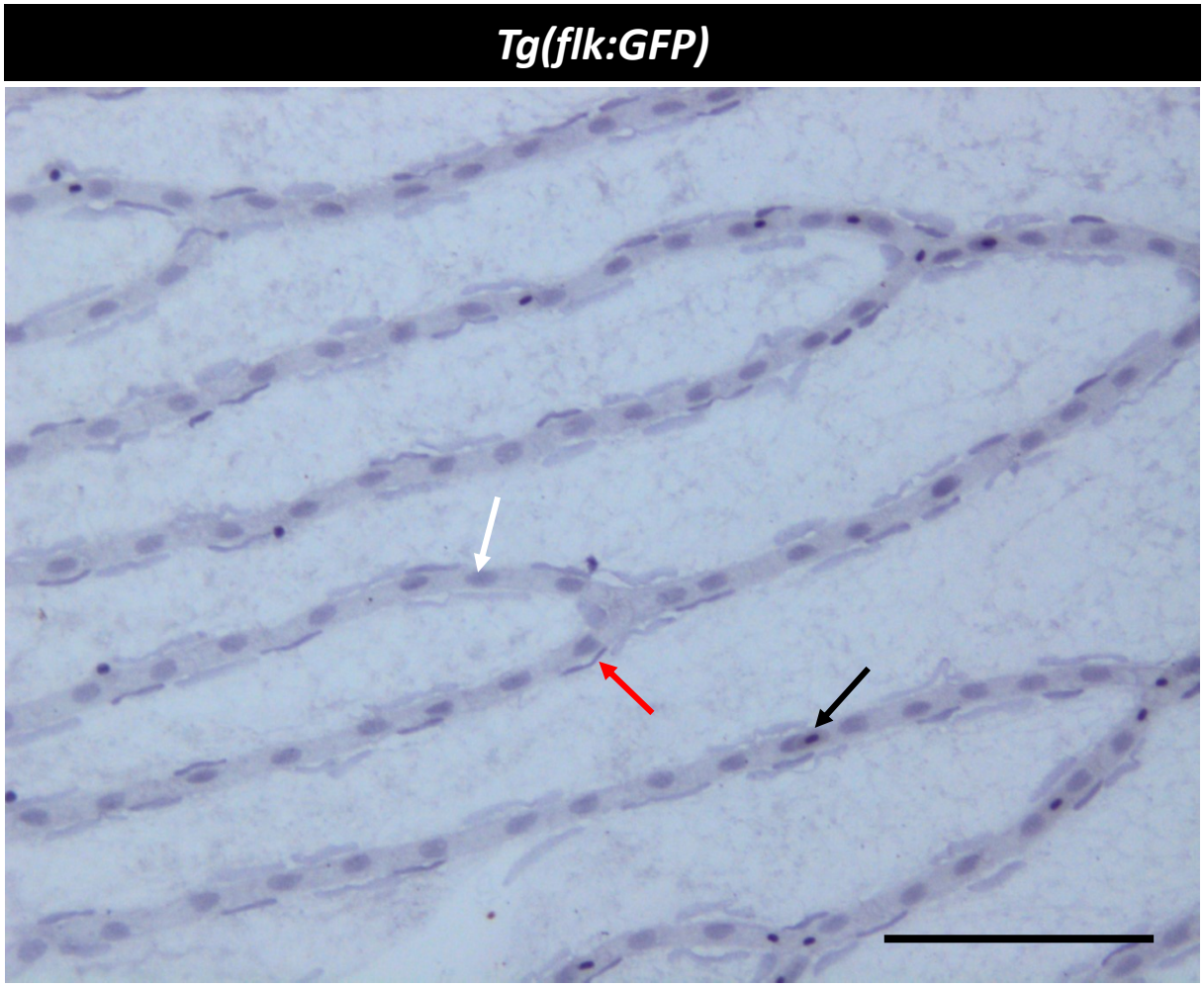

Figure 11: Trypsin digest of the zebrafish retina. 200x magnification of a zebrafish retinal trypsin digest preparation. Black arrow: erythrocyte. White arrow: endothelial cell. Red arrow: vascular mural cell. Scale bar: 100µm.

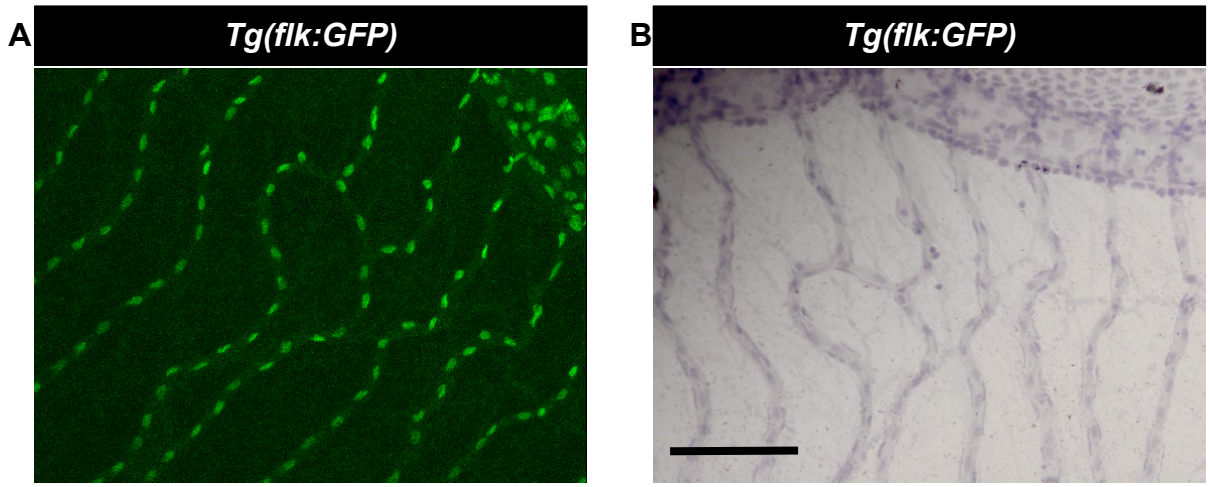

Figure 12: Identification of endothelial cells in the zebrafish retinal trypsin digest. A) Enlargement of a picture taken at 100x magnification of the retinal digest preparation of a Tg(flk:GFP) zebrafish using a fluorescence microscope. B) 200x magnification of the same retinal digest preparation after staining with haematoxylin. Scale bar: 100µm.

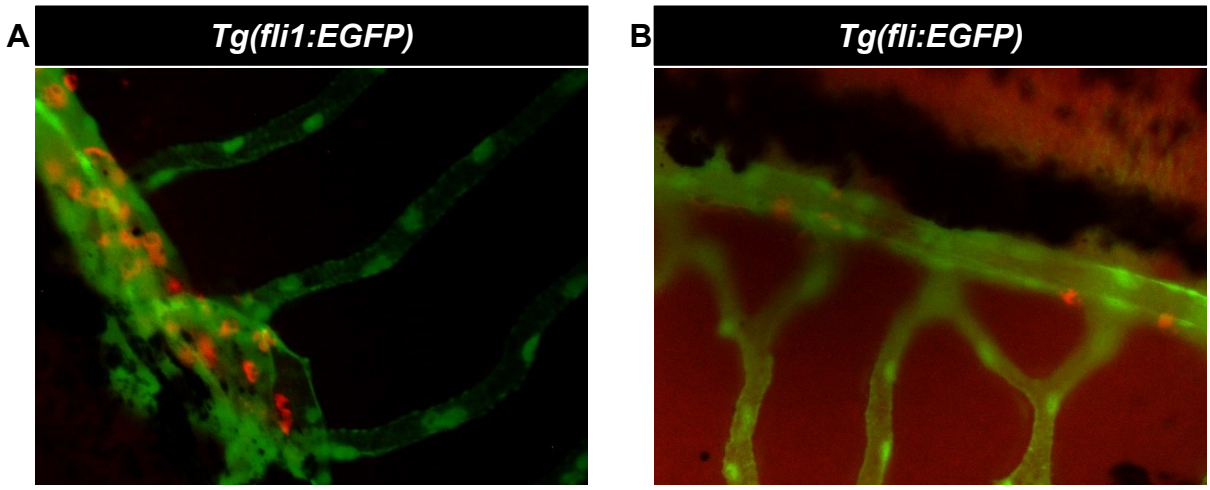

Figure 13: Antibody staining for pericytes. A) 400x magnification of Anti-NG2 antibody stain, counter stain with AF 594, in the retina of a transgenic *Tg(fli1:EGFP)* zebrafish. B) 400x magnification of Anti-PDGFRβ antibody stain, counter stain with TRITC, in the retina of a transgenic *Tg(fli1:EGFP)* zebrafish.

3.5.2 Analysis of the retinal vasculature in wildtype zebrafish

To establish how many endothelial cells and mural cells are expected to be found in adult wildtype zebrafish, we analysed six retinae of transgenic wildtype *Tg(flkn:GFP)* zebrafish at 20 months of age.

Furthermore, it was crucial to find out whether there are significant differences between different density areas of the retina. In zebrafish, the retina has four different areas characterized by vessel densities[80]. There is one high density, one low density and two medium density areas (Fig. 14). To account for potential differences in the different retinal areas, endothelial cells and pericytes were counted in each area.

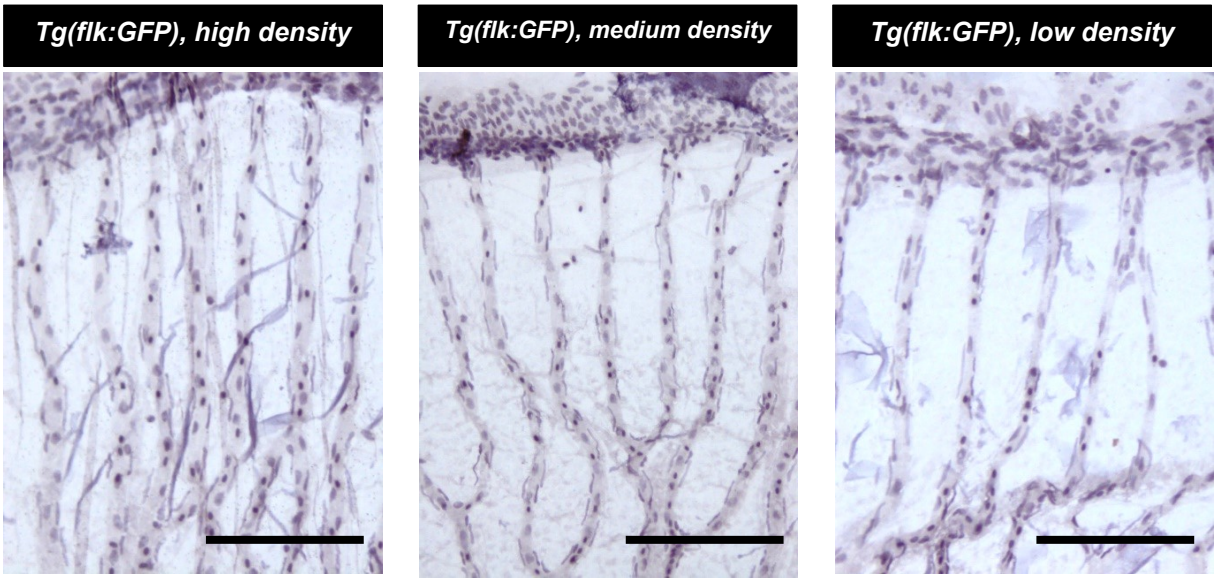

Figure 14: Representative images of the different areas of the retina (high density, medium density, low density) in the periphery. Scale bar: 100µm.

As the optic artery splits into five to seven main vessels which in turn split up two more times, we defined the main vessels before they split up as vessels in the central part of the retina, the vessels between the first and the second splitting point as vessels in the intermediate part of the retina and the vessels between the second splitting point and the IOC as vessels in the peripheral part of the retina. To establish how many endothelial cells and mural cells can be found in each part of the retina, I analysed the six retinae in 24 images each: One image of the vessels in the central part of the retina per area, two images of the vessels in the middle part of the retina per area and three images of the vessels in the peripheral part of the retina (Fig. 15). All images were taken at 200x magnification; endothelial cells and mural cells were counted on vessels of unperturbed identification of vascular cells over 200µm distance.

We found that there was no significant difference in the number of vessels or the average capillary area (µm^2) that could be analysed per image, the number of endothelial cells per mm^2 or the number of mural cells per mm^2 between the different areas (Table 1).

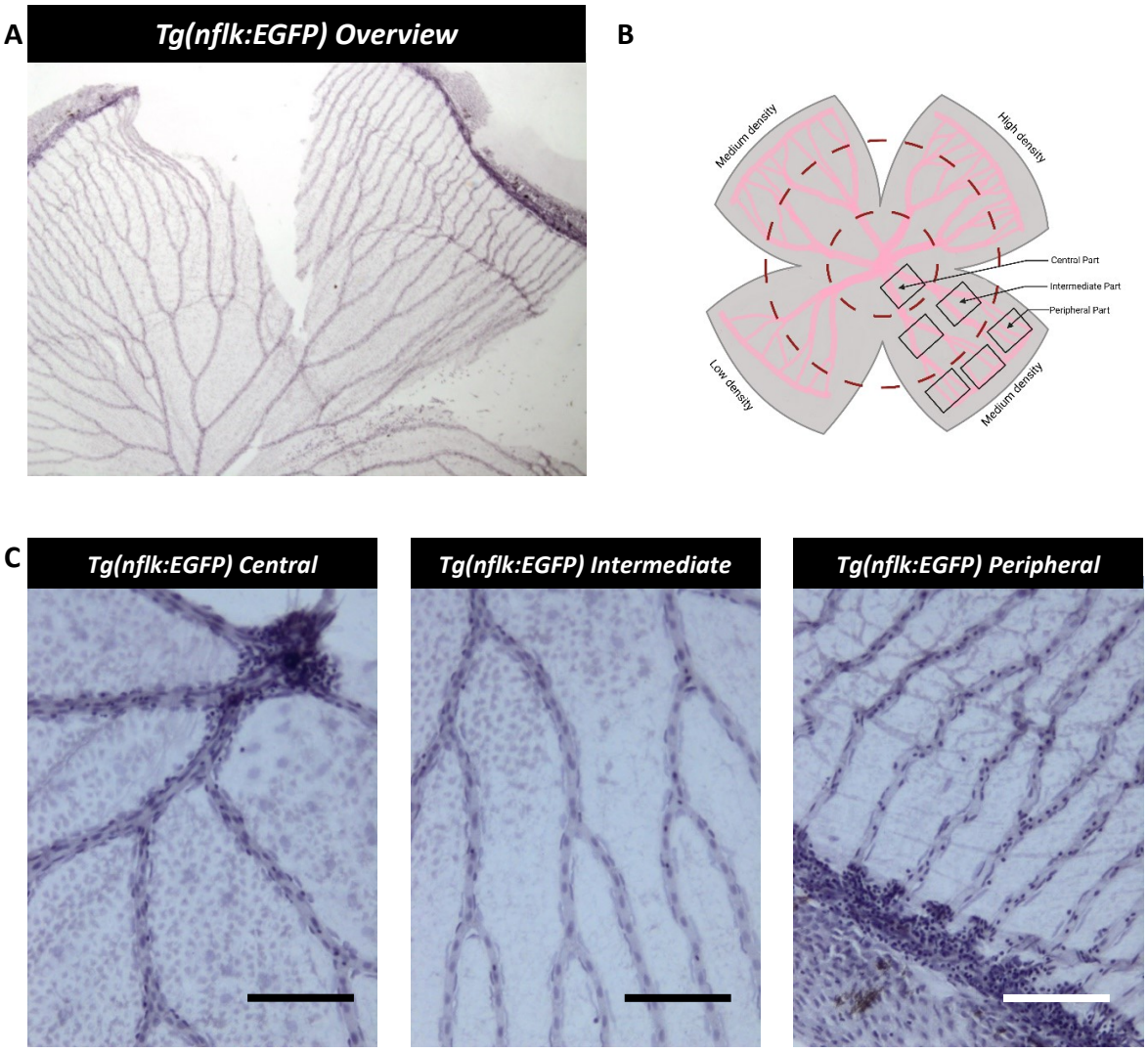

Figure 15: Analysis of the adult zebrafish retina according to density areas and distance to the entrance of the optic artery into the retina. A) Overview image of a retinal trypsin digest preparation, 40x magnification. B) Schematic overview of the areas analysed. C) Representative images of the different parts of the retina (central, intermediate, peripheral). Scale bar: 100µm. This figure was in part created with BioRender.com.

Part	High density area	Medium density area 1	Medium density area 2	Low density area
Number of vessels (average ± standard deviation)				
Central	2.67 ± 0.47	2.50 ± 0.76	2.33 ± 0.47	2.50 ± 0.50
Intermediate	3.17 ± 0.55	3.00 ± 0.95	3.31 ± 0.61	3.21 ± 0.67
Peripheral	4.22 ± 0.85	4.13 ± 0.81	4.00 ± 0.47	4.22 ± 0.53
Capillary area [µm²]/image (average ± standard deviation)				
Central	8048.67 ± 1961.70	7676.33 ± 2349.83	7200.67 ± 1873.63	7528.00 ± 2464.09
Intermediate	7902.85 ± 1000.5	7884.83 ± 2224.00	7767.62 ± 1292.67	7098.58 ± 1172.49
Peripheral	8455.30 ± 2034.50 0	8117.50 ± 1732.31	7829.95 ± 1185.63	8693.03 ± 1492.30
Endothelial cells/mm² (average ± standard deviation)				
Central	5053.96 ± 780.88	4343.28 ± 671.12	4736.18 ± 1004.80	4158.18 ± 423.75
Intermediate	4728.13 ± 715.98	4463.22 ± 427.15	4409.71 ± 810.19	4642.93 ± 603.73
Peripheral	4223.18 ± 876.44	4604.33 ± 542.89	4500.59 ± 853.14	4260.19 ± 1165.05
Mural cells/mm² (average ± standard deviation)				
Central	6559.54 ± 1159.17	6085.92 ± 502.25	6816.06 ± 1818.49	5939.32 ±706.03
Intermediate	6569.88 ± 850.76	5939.86 ± 942.83	6210.91 ± 1110.38	6689.00 ± 1193.11
Peripheral	4902.06 ± 833.77	5298.42 ± 1232.40	5234.32 ± 1534.50	5499.90 ± 1803.96

Table 1: Results of quantitative retinal morphometry in adult zebrafish.

Both the number of endothelial cells and the number of mural cells per mm^2 decreased from central to peripheral parts of the retina (Table 1). However, there was no difference in endothelial cell or mural cell numbers per mm^2 between the different areas when analysed in the same part (central, intermediate or peripheral) of the retina. This indicates that it is necessary to decide beforehand in which part the endothelial cells and mural cells are counted to ensure comparability between different experimental groups (Fig. 16).

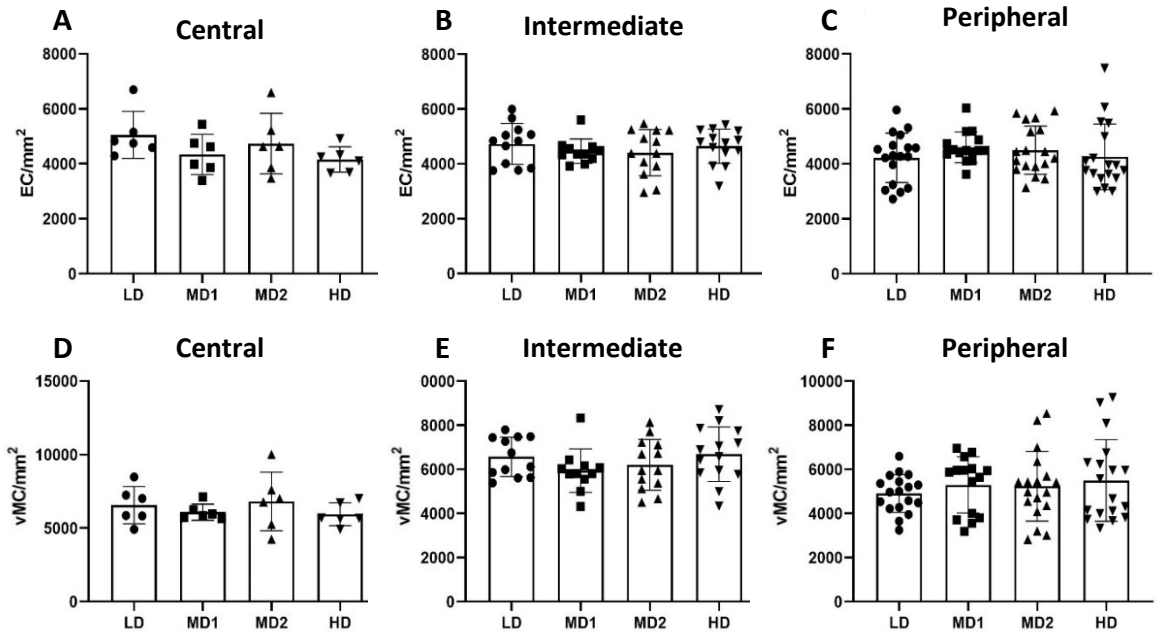

Figure 16: The number of endothelial cells and vascular mural cells per mm² do not vary between the different areas of the retina when calculated in the correlating parts. A, B and C) Number of endothelial cells per mm² in the central, intermediate, and peripheral parts of the retina according to density area. D, E and F) Number of vascular mural cells per mm² in the central, intermediate, and peripheral parts of the retina according to density area. Abbreviations: EC = endothelial cell, vMC = vascular mural cell, LD = low density area, MD1/2 = medium density area 1/2, HD = high density area.

The most reliably quantifiable part of the zebrafish retina was the intermediate part. In the central part, the high number of cells and the increased vessel diameter led to overlaps between the cells which made it difficult to decisively identify the different cell types. During preparation and digestion damage would sometimes occur in the peripheral part of the retina, which made analysing the same number of images per retina difficult. The middle part of the retina was usually well preserved, and the cells were spaced out along the vessel, making it easy to identify and quantify the different cell types.

To ensure comparability between zebrafish retinal digest preparations and mammalian retinal digest preparations it is necessary to calculate the number of endothelial cells and mural cells per mm². To calculate the capillary area in mm² the cells were counted over 200µm of vessel length and the vessel diameter was measured. While analysing the data we noticed that the vessel diameters vary between the different density areas in the intermediate part of the retina while they remain comparable in the central and peripheral part of the retina (Fig. 17). There are multiple reasons to use the intermediate part of the retina when performing a quantitative retinal morphometry. However, it is necessary to emphasize that the intermediate part of the retina is only suitable for analyses normalized to cells per mm² as in experimental groups the number of endothelial cells or mural cells per 200µm of vessel length may be the same while the numbers per mm² may be decreased or increased according to the difference in vessel diameter.

Furthermore, we found that the vessel diameter decreased from central to peripheral parts of the retina as well. In the central part of the retina, vessels had a diameter of

on average 15.13 ± 1.96µm, which decreased to 12.22 ± 1.61µm in the intermediate area and to 9.99 ± 1.12µm in the peripheral area. Therefore, only the vessels in the periphery of the retina qualify as capillaries, while the vessels in the intermediate and central parts of the retina should be considered arterioles.

As a general observation, we found that in the middle part of the retina, zebrafish have on average 6371.30 ± 1083.41 mural cells per mm^2 capillary area and 4563.20 ± 672.71 endothelial cells per mm^2 capillary area which translates to a mural cell to endothelial cell ratio of 1.4:1.

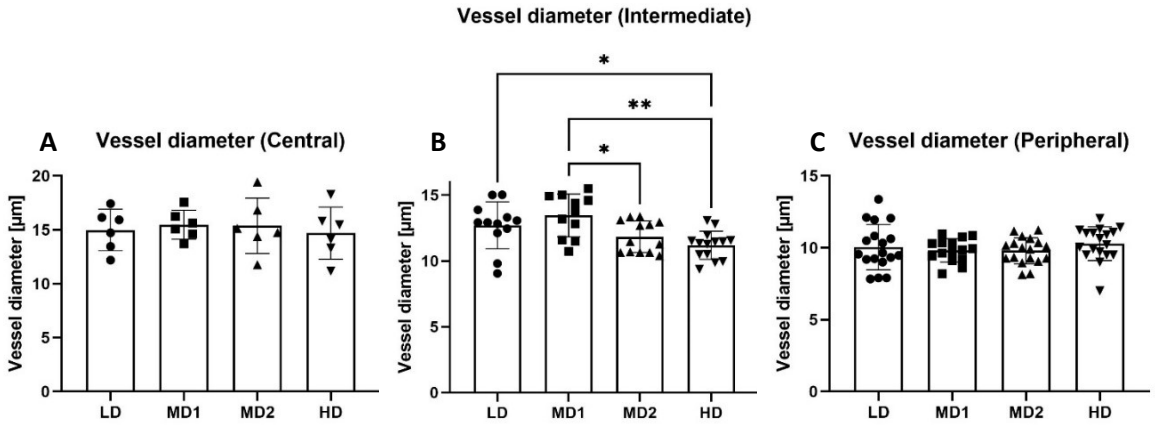

Figure 17: The vessel diameter varies between the different areas in the intermediate part of the retina. A, B and C) Vessel diameter [µm] in the different parts of the retina according to density areas. Abbreviations: LD = low density area, MD1/2 = medium density area ½, HD = high density area.

3.5.3 *pdx1*$^{+/-}$ mutants do not exhibit mural cell or endothelial cell loss

We analysed five retinae of each *pdx1*$^{+/-}$ zebrafish and their littermates. There was no relevant change in the number of mural cells or endothelial cells per mm^2 capillary area between the two groups (Fig. 18).
On average, *pdx1*$^{+/-}$ zebrafish had 3553.30 ± 583.59 endothelial cells and 5040.97 ± 748.09 mural cells per mm^2 capillary area while their littermates had 3519.06 ± 684.31 endothelial cells and 4976.38 ± 1075.60 mural cells per mm^2 capillary area.

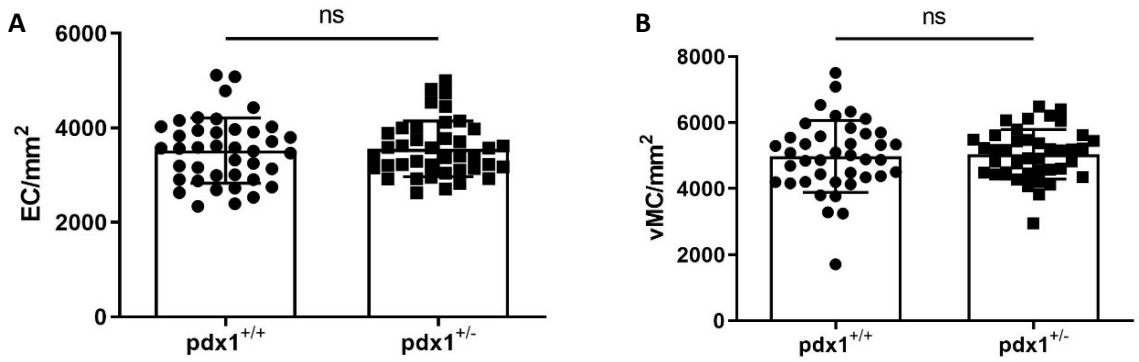

Figure 18: Number of endothelial cells and vascular mural cells/mm^2 in *pdx1*$^{+/-}$ zebrafish. A) EC/mm^2 in *pdx1*$^{+/-}$ zebrafish in comparison to their direct littermates. B) vMC/mm^2 in *pdx1*$^{+/-}$ mutants in comparison to their direct littermates. n=5 in both experimental groups.

3.5.4 *aldh2.1*$^{-/-}$ mutants exhibit relative mural cell loss in comparison to their littermates due to increased vessel diameter

We analysed five retinae of *aldh2.1*$^{-/-}$ zebrafish mutants and their littermates. Previous studies showed that aldehyde dehydrogenases (aldh) were upregulated in *glo1* mutants, indicating that aldehyde dehydrogenases may be involved in the methylglyoxal detoxification process[88]. Knockout of *aldh2.1* led to an angiogenic phenotype in the retina[77], and we therefore analysed the retinae utilizing the retinal trypsin digest protocol.

We found that adult *aldh2.1*$^{-/-}$ mutants had less vascular mural cells per mm^2 than their littermates (*aldh2.1*$^{-/-}$ mutants: 5202 ± 160.7 vMC/mm^2; littermates: 5801 ± 204.5 vMC/mm^2; p=0.0234), which could explain the angiogenic phenotype, as mural cell loss precedes angiogenesis in mammalian models of DR. However, the decreased numbers of vascular mural cells were not due to an absolute loss of mural cells but rather due to an increase in vessel diameter in the retinal vasculature of adult *aldh2.1*$^{-/-}$ mutants (*aldh2.1*$^{-/-}$ mutants: 10.81 ± 0.2126µm; littermates: 9.816 ± 0.1758; p=0.0006) and therefore an increase in vessel area in comparison to their littermates (Figure 19). This finding does not mean that a decreased coverage does not contribute to the angiogenic phenotype in the zebrafish retina, however, there is need for further research into the factors that lead to angiogenesis in the zebrafish retina.

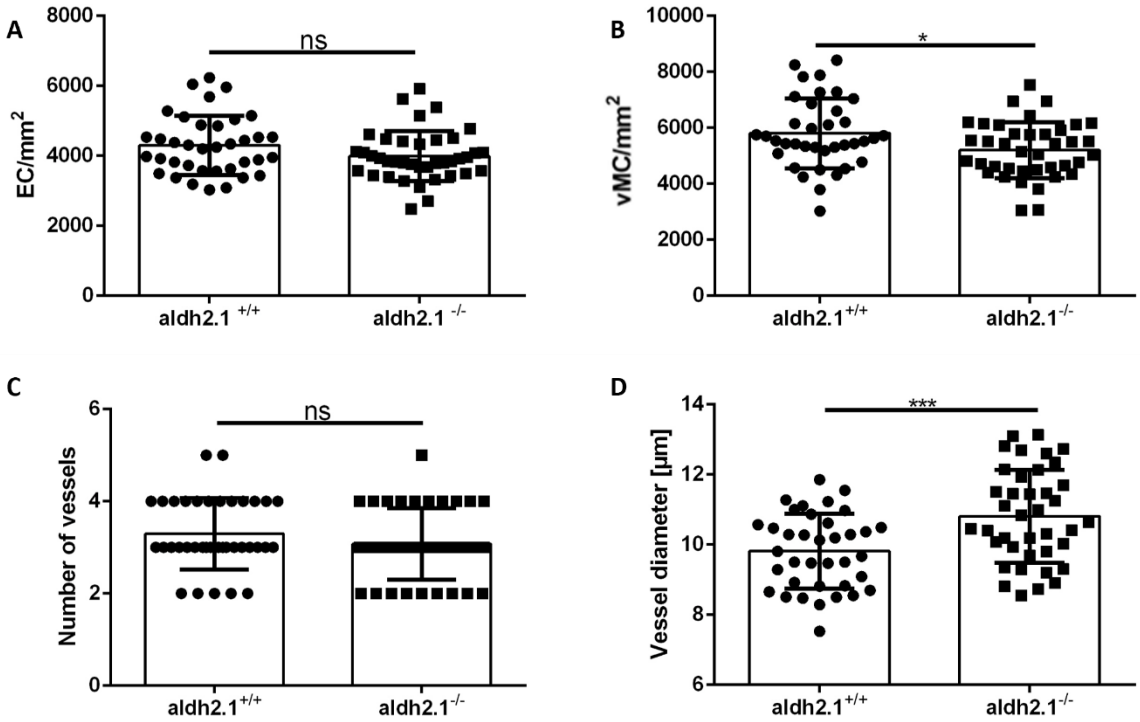

Figure 19: Difference in the numbers of vascular mural cells/mm² in *aldh2.1*$^{-/-}$ mutants. A) EC/mm² in *aldh2.1*$^{-/-}$ mutants in comparison to their littermates. B) Increased numbers of vMC/mm² in *aldh2.1*$^{-/-}$ mutants in comparison to their littermates. C) Number of vessels analysed in both experimental groups. D) Increased vessel diameter in *aldh2.1*$^{-/-}$ mutants in comparison to their littermates. n=5 in both experimental groups.

4 DISCUSSION

All components of the neurovascular unit can be identified in the zebrafish retina. Endothelial cells and vascular mural cells are present in the retinal vasculature and can be quantified using retinal trypsin digests. Müller glia and microglia are present and can be stained using GFAP and L-Plastin antibodies. The composition of the neuroretina is like that of the mammalian retina and an analysis of neurodegeneration can be performed using the paraffin slides. However, the results observed in this thesis indicate that the individual components in the retina of *pdx1*$^{+/-}$ zebrafish, which have been shown to react to high glucose levels through angiogenesis[31], do not interact in the way which has been extensively studied in the mammalian retina.

4.1 Studying neurodegeneration in a zebrafish model of retinal disease

During the comparison of the *pdx1* line with wildtype zebrafish, we found that comparison of retinal layer thickness can only produce reliable results when comparing zebrafish from the same mutant line, as the retinae from the *pdx1* line (of both heterozygous mutants and their wildtype littermates) were significantly thicker than those from the wildtype line.
Furthermore, we analysed the retinae of *pdx1*$^{+/-}$ zebrafish in comparison to those of their littermates at various points throughout their life cycle (at 4mpf, 12mpf and at 21mpf). We found that while at 4mpf, the overall retinal layer thickness of *pdx1*$^{+/-}$ zebrafish was significantly decreased in both central and peripheral parts of the retina in comparison to their wildtype littermates, this change was not reproducible at 12mpf or 21mpf, indicating that compensation of the phenotype takes place between the age of 4mpf and 12mpf in this zebrafish line.
Quantification of neuronal nuclei numbers was performed at all stages, however they did not provide evidence of a change in neuronal numbers except for an increase in neuronal nuclei in the periphery of the retina of *pdx1*$^{+/+}$ zebrafish at 12mpf. There was no increase in retinal layer thickness at the same timepoint. A possible explanation for this finding would be the regeneration of damaged neuronal cells, as the number of nuclei may increase temporarily due to the division of regenerating cells.
Neurodegeneration was one of the first pathologies to be analysed in zebrafish models of DR[24]. It was shown that in treated fish after 28 days of alternating immersion in glucose solution or water both the IPL and the INL were significantly thinner than in the control groups, leading researchers to consider zebrafish as a potential model to study DR[24].
However, further studies have not been able to produce reliable results when it comes to neurodegeneration in the zebrafish retina due to a diabetic phenotype. While significantly decreased IPL thickness was found in the glucose immersion-induced model described above[24] and in a model using STZ in zebrafish[89], another study described an increased IPL thickness in a model of immersion-induced hyperglycaemia (even though there was no change in the overall retinal thickness)[90] and in the genetic *pdx1* model there was an increase in nuclei in the INL[73].
All the above indicates that while short term effects of the influence of exposure to high glucose levels may lead to measurable changes in the retinal thickness of zebrafish, the effects in long-term models, such as mutant lines, are not easily reproduced. This is most likely due to the regenerative capabilities of the zebrafish retina. The results from our study described above contribute to this observation.

Signs of neurodegeneration in the form of changes in retinal layer thickness and neuronal nuclei numbers can be measured in zebrafish in analogy to mammalian models of DR. However, genetic zebrafish models are not likely to show reproducible signs of neurodegeneration. While it is possible that prolonged and intense exposure to high glucose levels can produce a phenotype that resembles neurodegeneration as described above[24], genetic models without long periods of exposure to high glucose but with blood glucose levels that only increase postprandially do not seem to have a neurodegenerative phenotype. A potential explanation could be that the regenerative capabilities of the zebrafish retina make it impossible to quantify neurodegeneration, since the retinal layer thickness and the number of nuclei changes dynamically throughout the time of the experiment. Furthermore, as demonstrated experimentally, the number of nuclei can vary without any effect to the thickness of the related retinal layer (for details, see chapter 3.1.4). This explanation might not be applicable to the glucose immersion-induced model, as the intense effect of glucose might be able to suppress the regenerative capabilities of the zebrafish retina during the short time of the experiment; however, this has not been studied so far and is only a hypothesis at this point.

4.2 Proliferation is not increased in *pdx1*$^{+/-}$ mutants

We analysed the retinae of *pdx1*$^{+/-}$ zebrafish for signs of proliferation by using an antibody stain for PCNA. We could find no increase in PCNA positive cells in either the retinae of *pdx1*$^{+/-}$ or the retinae of *pdx1*$^{-/-}$ mutants in comparison to their littermates. Most of the PCNA positive cells in our experiments were in the ONL, which could indicate that there is a constant low level of damage leading to the formation of neuronal progenitor cells (NPCs) in the retinae of the fish; however, since both mutants and littermates are affected equally this is unlikely to be because of high glucose.
As reviewed extensively, teleost fish such as zebrafish have the capability to regenerate all cell types of the retina after damage[91-93]. Even though the reasons for this potential and why teleost fish have this capacity while mammals do not are still unclear, the mechanisms and events that occur within the zebrafish retina during damage and regeneration have been studied broadly in recent years.
In general, dying neurons stimulate Müller glial dedifferentiation and acquisition of stem cells properties as well as proliferation which leads to the generation of neuronal progenitor cells (NPCs) and their migration to the damaged retinal layers where they regenerate the neuronal cell types that were lost.[93] Changes in gene expression[94] and partial reprogramming of the genome characterized by changes in DNA methylation and activation of genes associated with multipotency[95] are part of the regenerative process.
The cell bodies of Müller glial cells are usually positioned in the INL, however, the formation of NPCs occurs through asymmetrical division of Müller glial cells in the ONL. This migration during the regenerative process is referred to as interkinetic nuclear migration[96]. There are various known genetic markers that are expressed by Müller glial cells during the dedifferentiation process they undergo during the regenerative process in the zebrafish retina. One of the first markers expressed by the NPCs is PCNA, which is shown by an increased number of PCNA positive cells in the ONL[94]. PCNA is therefore used in zebrafish to quantify proliferation and thereby regeneration after a sustained injury[97].
Our finding of PCNA positive cells in the ONL is therefore in accordance with the available evidence on the process of regeneration in the zebrafish retina. In the retinae of

pdx1$^{+/-}$ or *pdx1*$^{-/-}$ zebrafish there is no increase of proliferation above the expected levels.

4.3 Müller glial cells do not undergo morphological changes indicative of reactive gliosis in the retinae of *pdx1*$^{+/-}$ mutants

Müller glial cells were visualized using a GFAP stain. While establishing the protocol to confirm the occurrence of Müller glia activation in zebrafish, we found that GFAP positive cells were present in the retinae of wildtype zebrafish. This is an interesting finding, as in mammalian models of DR or human diabetic patients GFAP gets upregulated because of hyperglycaemia and indicates Müller glia activation.
We hypothesized that Müller glia activation in zebrafish could be shown by analysing the retina for morphological changes in the GFAP positive cells or by quantifying the cells. However, we did not identify any clear morphological changes in the retinal sections and did not find an increased number of GFAP positive cells per retina between the different groups.
At 12mpf, zebrafish from the *pdx1*$^{+/+}$ line that descends from two *pdx1*$^{+/+}$ parents showed an increased number of GFAP positive cells. The same fish had an increased number of neuronal nuclei in the INL, indicating that there may be some form of increased regeneration in progress in this *pdx1*$^{+/+}$ line in comparison to the *pdx1*$^{+/-}$ mutants and their direct littermates.
Other researches have seen morphological changes in the retinae of *pdx1*$^{-/-}$ zebrafish after staining for glutamine synthetase (GS)[73].
Apart from their role in the regeneration of the zebrafish retina, Müller glia have long been implicated in the pathogenesis of DR in animal models and diabetic patients[98]. Their processes reach across the entire span of the retina, with their end feet reaching both the ganglion cells and blood vessels at the inner limiting membrane and the photoreceptors in the outer segment of the retina[50].
Müller cells possess multiple characteristics that indicate their involvement in DR. They are involved in glucose uptake and phosphorylation in the retina[99] and carry the glucose transporter GLUT1[100], through which glucose can be transported into the cell without insulin regulation. Müller cells metabolize glucose through glycolysis, store glucose in the form of glycogen and are endowed with the enzyme aldose reductase[101], making them susceptible to the consequences of the polyol pathway. They are furthermore involved in the potassium, glutamate and GABA metabolism of the retina and possess the enzyme glutamine synthetase (GS)[102].
As mentioned above, they are in close contact with every other cell in the retina. Müller cell dysfunction contributes to all major pathologies associated with DR: photoreceptor and neuronal degeneration, breakdown of the BRB and intraretinal neovascularization[98].
During the pathogenesis of DR, Müller cells first become activated, which has been reviewed extensively[98, 103]. The main marker used for the detection of Müller glial activation (also referred to as reactive gliosis) is GFAP. Other markers for Müller glial cells include GS and Bcl-2, however it has been shown that in human diabetic patients GFAP is upregulated in comparison to non-diabetic controls, while the distribution and intensity of GS and Bcl-2 remain the same[104]. As described above, to detect evidence for Müller glial activation in zebrafish it is necessary to regard the morphology of the Müller glia rather than the sole expression of a marker protein. To that end, according to the evidence published so far[73], in zebrafish it is irrelevant whether GFAP or GS is used to mark Müller cells.

In conclusion, we have shown that while in the mammalian retina reactive gliosis can be quantified by immunohistochemical detection of GFAP expression, this is not the case in zebrafish. It is likely that the Müller glial cells in the zebrafish retina are activated as well, however, this does not depend on the genotype or the occurrence of hyperglycaemia. As Müller cells play an essential role in regeneration in the zebrafish retina, it is likely that the constant activation is in relation to this process.

4.4 Microglia activation is not increased in *pdx1*$^{+/-}$ mutants

In our experiments, we used the L-Plastin stain, which is often used in zebrafish research. After inducing damage to the retina, researchers have found that L-Plastin positive cells increase in numbers and cluster around the injured area[105]. We found that the L-Plastin positive cells in the retinal sections were at the borders of the plexiform layers and in the ganglion cell layer, which lays directly below the inner limiting membrane and the retinal vasculature. However, there was no increased number of L-Plastin positive cells in any of the experimental groups. We found various clusters of L-Plastin positive cells in the OPL, the GCL or at the optic nerve entrance into the retina, which are all expected locations of microglial infiltration due to the data available from mammalian models. However, these clusters were not increased in any of the experimental groups but were found in all groups equally.
Microglia are the resident macrophages in the retina and are located in the GCL, both plexiform layers and around the retinal vessels[50]. Under normal circumstances, microglia are programmed for immunotolerance and are controlled through anti-inflammatory cytokines such as transforming growth factor (TGF)-β, which gets released by the healthy RPE. Once activated, microglia can protect neurons from cell death by removing toxic by-products and cell debris; chronic activation however leads to secondary tissue damage[106]. In early stages of human diabetic retinopathy microglia become hypertrophic in all retinal layers and increase slightly in numbers around the vasculature before they start infiltrating the optic nerve region. During PDR, they cluster heavily around dilated new vessels[107]. We found microglia in the areas that were expected from mammalian models of DR. However, there was no increase in L-Plastin positive cells in the *pdx1*$^{+/-}$ zebrafish in comparison to their littermates.
At present, there are no studies on microglia or inflammatory processes in zebrafish models of DR. Our findings suggest that microglia may not play a role in the pathogenesis of DR in zebrafish.

4.5 Quantitative retinal morphometry in zebrafish

One of the main contributions to current research that we performed in our study was the adaption of the retinal digest protocol to the zebrafish retina and the identification of the different cell types visible in the preparations. This enables future researchers to analyse their zebrafish models of retinal disease for pathologies including endothelial cell loss, mural cell loss and vessel dilation.
We adapted the established protocol[83] to the zebrafish retina (for details, see chapter 2.2.3). We identified endothelial cells by using the transgenic *Tg(nflk:GFP)* zebrafish line[76]. Mural cells and erythrocytes were identified through literature research[86, 108].
We counted mural cells and endothelial cells in six adult zebrafish retinae in central, intermediate and peripheral parts of the retinae. We considered the different density areas of the zebrafish retina and compared the cell numbers according to their density area. To ensure comparability to other models of retinal pathologies, we calculated the

cell numbers as cells per mm^2 by counting the cells over 200µm of vessel length and then calculating the vessel area using the vessel diameter, which we measured as well.
We found that endothelial cells and mural cells have distinct morphologies and locations in the zebrafish retinal trypsin digest preparation which can be identified reproducibly. Endothelial cells have oval nuclei which are in the middle of the vessel and after staining with Mayer's haemalum solution take on a light purple colour. Mural cells have long and flat nuclei which are located on top of vessels and take on a dark purple colour. There is a slight gap between the vessel wall and the nuclei of the mural cells. This is in analogy to the mammalian retina, where pericytes occupy the "pericyte niche" inside the basal membrane[59]. The last kind of nuclei, which are small, round and very dark and can be found both inside and around the vessels, most likely belong to erythrocytes, since zebrafish erythrocytes have nuclei in contrast to mammalian erythrocytes[86].
We found that there is no difference in endothelial cell or mural cell numbers per mm^2 regarding the density areas. Comparing central, intermediate and peripheral parts of the retina, we found that endothelial cell and mural cell numbers decline significantly from the central to the peripheral part of the retina.
We found that in the intermediate part of the retina, the vessel diameter varies between the different density areas. This was a relevant finding, as this indicated that the cell numbers should be calculated as cells per mm^2 to account for potential differences in cell coverage which would not be quantified if the cells were presented as cells per vessel length.
Furthermore, we found that the vessel diameter declined from central to peripheral parts of the retina, indicating that only peripheral parts of the retinal vasculature can be considered capillaries. This has been described before[109]. It has been described that vascular mural cells change their phenotype in the form of their morphology and marker expression dependent on which vessel type they are associated with[110]. Typically, arterioles are covered by vascular smooth muscle cells (vSMC). On precapillary arterioles, smooth muscle-pericyte hybrids can be found and definite pericytes can only be found on capillaries[110].
Many pathologies associated with DR are caused by the loss of pericytes and endothelial cells in the retina. Dropout of pericytes and endothelial cells is implicated in the formation of acellular capillaries which can no longer provide blood flow to parts of the retina, leading to an ischaemic state. To combat the hypoxia, various cell types of the retina including Müller cells start excreting angiogenic factors such as Angiopoietin (Ang-)2 and VEGF leading to intraretinal neovascularization[10].
Although not generally recognized as a factor in the pathogenesis of DR, vSMC and arterioles have been found to be affected by hyperglycaemic conditions as well[111, 112]. The appearance of vSMC "ghosts" can be found in retinal trypsin digests in analogy to pericyte ghosts, which indicate pericyte loss in capillaries[111]. Apart from vSMC loss, persistent dilation of retinal arterioles has been observed in diabetes as well, which may lead to increased retinal blood flow and represent arteriolar dysfunction[111].
Before our study, it had been shown through electron microscopic analysis of the ultrastructure of retinal vessels that pericytes exist in the zebrafish retina[59] and that they express PDGFRβ[87, 113] and Notch3[114]. Furthermore, in the *pdx1*$^{-/-}$ model of DR it was shown that mutants express less Transgelin1 than controls from the age of 3 mpf onwards[73]. However, Transgelin1 is not a specific marker for pericytes. It is an early marker for vascular mural cells (vMC) in general[115], further indicating that vMC may be affected by hyperglycaemic conditions as well.

Applying this protocol, we performed an analysis of the retinal vasculature on the *aldh2.1*$^{-/-}$ zebrafish line. Aldehyde dehydrogenases (Aldh) are an enzyme family which are involved in the detoxification of various reactive metabolites. Loss of *aldh2* in humans and rats leads to an increase in reactive oxygen species (ROS). The zebrafish homolog to human *aldh2* is *aldh2.1*[77]. Using the retinal digest protocol, we could show that there was a decrease of mural cell coverage in the retinal arterioles of 10%, while endothelial cell numbers remained unchanged. Furthermore, we could show that the vessel diameter of the retinal arterioles was significantly increased[77].
We applied the protocol to the retinae of *pdx1*$^{+/-}$ zebrafish as well. However, we could find no decrease in endothelial or mural cell numbers. Previous work from our group had shown that *pdx*$^{-/-}$ and *pdx1*$^{+/-}$ zebrafish show an increased sprout and branch formation at 20mpf after periods of postprandial hyperglycaemia[31]. This is an interesting observation, as mural cell dropout precedes neovascularization in the mammalian retina. It was shown that the neovascularization in *pdx1*$^{-/-}$ zebrafish is accompanied by increased VEGF mRNA expression and can be rescued by incubation with a VEGF-receptor inhibitor, suggesting that the mechanism of neovascularization in the zebrafish retina has pathophysiological similarities with the formation of new blood vessels during PDR[31]. Furthermore, it was shown that in the retinae of *pdx1*$^{-/-}$ zebrafish the integrity of the BRB is impaired, leading to vessel leakage[73]. How these pathologies can occur without previous mural cell or endothelial cell dropout is an observation which requires further investigation, as it implies that the pathogenesis of microvascular dysfunction in the zebrafish retina may be dependent on other factors than in the mammalian retina.
In conclusion, we successfully performed the adaptation of the retinal trypsin digest protocol to the zebrafish retina, which will help future researchers in the field analyse the zebrafish retina for signs of endothelial and mural cell loss as well as vessel dilation.

4.6 Conclusion: The Neurovascular Unit in the zebrafish retina

We have completed an analysis of the neurovascular unit in the zebrafish retina with all its components. All components could be identified and quantified in the zebrafish retina. However, we could not find any evidence that the individual components in the retinae of *pdx1*$^{+/-}$ zebrafish interacted in the way that we expected from the mammalian retina, even though the *pdx1* zebrafish mutant line has become a well-regarded model for diabetic microvascular complications[31, 72, 73, 116].
This could be because the *pdx1*$^{+/-}$ zebrafish line does not suffer from chronic hyperglycaemia with an increased HbA_1c but rather from postprandial episodes of hyperglycaemia. However, it may also be because the retinal vasculature in zebrafish shows many dissimilarities to the mammalian retina.
One of the key differences between the zebrafish and the mammalian retinal vasculature is its position within the retina. The blood supply in the mammalian retina is provided by two vascular plexuses, the choroid and the intraretinal plexus. In physiological conditions, all vessels remain underneath the ILM and it is a sign of pathological neovascularization if vessels break through the ILM and into the vitreous cavity. Zebrafish only have one network of retinal vessels, and it is located on top of the ILM. Vessels do not reach into the retina and are therefore not in direct contact with any of the other components of the neurovascular unit except for Müller glia end feet. It is therefore worth considering that in zebrafish the retinal phenotype we can observe in diabetic conditions may not be dependent on the interactions of the individual components of the neurovascular unit.

5 SUMMARY

In recent years, zebrafish *(Danio rerio)* have become an established model to study retinal diseases. Most of the research in zebrafish has focused on vascular and neuronal pathologies. However, in many retinal diseases, such as diabetic retinopathy, the entirety of the neurovascular unit, which includes retinal neuronal cells, retinal macroglia (especially Müller glial cells) and microglia and retinal vascular cells (endothelial cells and vascular mural cells/pericytes), is disrupted.
Therefore, this study aimed to analyse whether all components of the neurovascular unit are present in the zebrafish retina and to establish methods which can be used to analyse the neurovascular unit in the zebrafish retina. Those methods were then used to analyse the retinae of *pdx1*$^{+/-}$ zebrafish mutants, which have gained interest as a potential model for pathologies associated with diabetic retinopathy.
The methodical approach to analyse loss of neuronal cells in mammalian retinae could be performed on zebrafish without alterations of the protocol. The retinae of *pdx1*$^{+/-}$ zebrafish were analysed at three different time points throughout adulthood: 4 months post fertilization (mpf), 12mpf and 20mpf. At 4mpf and 12mpf the overall retinal layer thickness was decreased. However, this change did not persist until 20mpf, which indicated that some form of regeneration was taking place in the zebrafish retina, making it difficult to evaluate potential changes.
To analyse whether there were signs of regeneration, we performed an antibody stain for PCNA (proliferating cell nuclear antigen), an established marker for proliferation in the zebrafish retina. However, there was no increase in proliferating cells in the retinae of *pdx1*$^{+/-}$ zebrafish.
We found that while in mammals Müller glia only express glial fibrillary acidic protein (GFAP) once they become activated, in zebrafish Müller glia cells always express GFAP. Therefore, to evaluate whether there was increased Müller glial activation, we had to modify the established protocol. Instead of analysing whether Müller glia express GFAP, we counted and compared the number of GFAP-positive cells. In the *pdx1*$^{+/-}$ retina, we could find no difference between mutants and controls.
L-Plastin was used as a marker to identify microglia. There was no increase in L-Plastin positive cells in the retinae of *pdx1*$^{+/-}$ zebrafish.
Previous work has shown angiogenesis in the *pdx1*$^{+/-}$ retina at 18mpf. To evaluate whether the vascular cells were affected to explain this phenomenon, we adapted the retinal trypsin digest protocol to the zebrafish retina. After identification of the different cell types which are visible in the zebrafish retinal trypsin digest preparation the average number of endothelial cells and vascular mural cells per square millimetre in the adult zebrafish retina were established. However, in comparison to controls, *pdx1*$^{+/-}$ mutants did not suffer any pericyte or endothelial cell loss.
In conclusion, we can show that all components of the neurovascular unit which have been identified in the mammalian retina are present in zebrafish as well. However, at least in the *pdx1*$^{+/-}$ zebrafish line, they do not seem to interact in a way that would be expected from mammalian models. This indicates that the reaction of the zebrafish retina to hyperglycaemic environmental conditions most likely differs from mechanisms known from mammalian models and needs further investigation. To facilitate future work on the zebrafish retina, this thesis provides detailed and comprehensive protocols to analyse the retinal neurovascular unit in the zebrafish retina.

6 ZUSAMMENFASSUNG

Der Zebrafisch *(Danio rerio)* ist in den letzten Jahren ein etabliertes Tiermodell für Netzhauterkrankungen geworden. In einem Großteil der Studien wurde hierbei der Fokus auf vaskuläre und neuronale Pathologien gelegt. Bei vielen Netzhauterkrankungen, wie beispielsweise der diabetischen Retinopathie, ist allerdings bekannt, dass die gesamte neurovaskuläre Einheit, bestehend aus Neuronen, retinalen Makro- (insbesondere Müller Glia) und Mikroglia sowie den Zellen der Blutgefäßwand (Endothelzellen und Gefäßwandzellen/Perizyten), von den Veränderungen betroffen ist.
Diese Dissertation hatte dementsprechend das Ziel herauszufinden, ob alle Zellen der neurovaskulären Einheit auch in der Zebrafisch Retina vorhanden sind, sowie Methoden zu etablieren, die im Zebrafisch verwendet werden können, um die neurovaskuläre Einheit in der Retina zu analysieren. Diese Methoden wurden danach angewandt, um die Retinae von *pdx1*$^{+/-}$ Zebrafischmutanten zu analysieren, da diese Mutante in den letzten Jahren als potenzielles Tiermodell für diabetische Retinopathie etabliert wurde.
Das Protokoll, das in den Retinae von Säugetieren verwendet wird, um den Verlust von Neuronen darzustellen, konnte ohne Veränderungen für den Zebrafisch übernommen werden. Es wurden Retinae von *pdx1*$^{+/-}$ Zebrafisch zu unterschiedlichen Zeitpunkten untersucht (4 Monate nach der Fertilisation (mpf = months post fertilisation), 12mpf und 20mpf). Die Dicke der Gesamtretina war sowohl zum Zeitpunkt 4mpf als auch zum Zeitpunkt 12mpf bei *pdx1*$^{+/-}$ Zebrafischen verringert. Diese Veränderung war zum Zeitpunkt 20mpf nicht mehr nachweisbar, was wiederum dafürspricht, dass dazwischen Regeneration stattgefunden haben muss. Dementsprechend ist es im Zebrafisch schwierig, potenzielle Zeichen der Neurodegeneration abzubilden.
Für den Nachweis von proliferierenden Zellen in der Retina wurde der etablierte Marker „proliferating cell nuclear antigen“ (PCNA) verwendet. In der Retina von *pdx1*$^{+/-}$ Mutanten konnte keine erhöhte Rate an proliferierenden Zellen festgestellt werden.
Bei der Analyse der Müller Glia stellten wir fest, dass im Gegensatz zu Säugetieren, deren Müller Glia den Marker „glial fibrillary acidic protein“ (GFAP) nur exprimieren, wenn sie aktiviert sind, die Müller Glia in der Zebrafischretina dauerhaft GFAP exprimieren. Um dennoch feststellen zu können, ob die Müller Glia in der Zebrafischretina aktiviert waren, modifizierten wir das im Säugetier etablierte Protokoll. Um einen Vergleich zwischen den Gruppen zu ermöglichen, zählten wir die GFAP positiven Zellen in den jeweiligen Gruppen. Bei der *pdx1*$^{+/-}$ Zebrafischlinie konnten wir keinen Unterschied in der Anzahl der GFAP-positiven Zellen zwischen Mutanten und Kontrollen feststellen.
Als Marker für die Identifikation von Mikroglia wurde L-Plastin verwendet. In den Retinae von *pdx1*$^{+/-}$ Zebrafischen waren nicht mehr L-Plastin positive Zellen zu finden als in der Kontrollgruppe.
In der Retina von *pdx1*$^{+/-}$ Zebrafischen wurde bereits nachgewiesen, dass verstärkte Angiogenese ab dem Alter von 18mpf festgestellt werden kann. Um quantifizieren zu können, ob die Zellen der Gefäßwände im Zebrafisch beeinträchtig waren, wurde das Digestionsprotokoll, das in der Säugerretina regelhaft verwendet wird, auf den Zebrafisch angepasst. Die Endothelzellen und Gefäßwandzellen wurden identifiziert und es wurde ausgewertet, wie viele Endothelzellen und Gefäßwandzellen normalerweise in der adulten Zebrafischretina pro Quadratmillimeter vorkommen. Im Vergleich zur Kontrollgruppe konnte bei *pdx1*$^{+/-}$ Zebrafischen kein Endothelzell- oder Gefäßwandzellverlust nachgewiesen werden.

In dieser Arbeit konnten wir zeigen, dass alle beteiligten Zellen der neurovaskulären Einheit, die aus der Retina von Säugetieren bekannt sind, auch in der Retina von Zebrafischen vorkommen. Allerdings scheint es, als würden sie zumindest in der *pdx1*$^{+/-}$ Zebrafischlinie nicht so interagieren, wie dies von Experimenten in Säugetieren zu erwarten wäre. Dies ist ein Hinweis, dass die Reaktion der Zebrafischretina auf Umgebungseinflüsse wie Hyperglykämie eventuell anders ausfällt als dies aus der Retina von Säugetieren bekannt ist. An dieser Stelle ist weitere Forschung von Nöten. Um zukünftige Arbeiten an der Zebrafischretina zu erleichtern, werden mit dieser Dissertation detaillierte und nachvollziehbare Protokolle zur Verfügung gestellt, um die Komponenten der retinalen neurovaskulären Einheit zu analysieren.

7 REFERENCES

1. Ogurtsova K, da Rocha Fernandes JD, Huang Y, Linnenkamp U, Guariguata L, Cho NH, et al.: IDF Diabetes Atlas: Global estimates for the prevalence of diabetes for 2015 and 2040. *Diabetes Res Clin Pract,* 128**:** 40-50, 2017 10.1016/j.diabres.2017.03.024
2. American Diabetes A: Diagnosis and classification of diabetes mellitus. *Diabetes Care,* 36 Suppl 1**:** S67-74, 2013 10.2337/dc13-S067
3. Zimmet P, Alberti KG, Shaw J: Global and societal implications of the diabetes epidemic. *Nature,* 414**:** 782-787, 2001 10.1038/414782a
4. Forbes JM, Cooper ME: Mechanisms of diabetic complications. *Physiol Rev,* 93**:** 137-188, 2013 10.1152/physrev.00045.2011
5. Harding JL, Pavkov ME, Magliano DJ, Shaw JE, Gregg EW: Global trends in diabetes complications: a review of current evidence. *Diabetologia,* 62**:** 3-16, 2019 10.1007/s00125-018-4711-2
6. Solomon SD, Chew E, Duh EJ, Sobrin L, Sun JK, VanderBeek BL, et al.: Diabetic Retinopathy: A Position Statement by the American Diabetes Association. *Diabetes Care,* 40**:** 412-418, 2017 10.2337/dc16-2641
7. Antonetti DA, Silva PS, Stitt AW: Current understanding of the molecular and cellular pathology of diabetic retinopathy. *Nat Rev Endocrinol*, 2021 10.1038/s41574-020-00451-4
8. Fundus photographic risk factors for progression of diabetic retinopathy. ETDRS report number 12. Early Treatment Diabetic Retinopathy Study Research Group. *Ophthalmology,* 98**:** 823-833, 1991
9. Stewart JM, Coassin M, Schwartz DM: Diabetic Retinopathy. In: *Endotext.* edited by Feingold KR, Anawalt B, Boyce A, Chrousos G, de Herder WW, Dhatariya K, et al., South Dartmouth (MA), 2000,
10. Hammes HP, Feng Y, Pfister F, Brownlee M: Diabetic retinopathy: targeting vasoregression. *Diabetes,* 60**:** 9-16, 2011 10.2337/db10-0454
11. Grading diabetic retinopathy from stereoscopic color fundus photographs--an extension of the modified Airlie House classification. ETDRS report number 10. Early Treatment Diabetic Retinopathy Study Research Group. *Ophthalmology,* 98**:** 786-806, 1991
12. Gardner TW, Larsen M, Girach A, Zhi X, Protein Kinase CDRSSG: Diabetic macular oedema and visual loss: relationship to location, severity and duration. *Acta Ophthalmol,* 87**:** 709-713, 2009 10.1111/j.1755-3768.2009.01545.x
13. Samuels IS, Bell BA, Pereira A, Saxon J, Peachey NS: Early retinal pigment epithelium dysfunction is concomitant with hyperglycemia in mouse models of type 1 and type 2 diabetes. *J Neurophysiol,* 113**:** 1085-1099, 2015 10.1152/jn.00761.2014
14. Group TASGaAES: Effects of Medical Therapies on Retinopathy Progression in Type 2 Diabetes. *New England Journal of Medicine,* 363**:** 233-244, 2010 10.1056/NEJMoa1001288
15. Kohner EM, Stratton IM, Aldington SJ, Holman RR, Matthews DR, Group UKPDS: Relationship between the severity of retinopathy and progression to photocoagulation in patients with Type 2 diabetes mellitus in the UKPDS (UKPDS 52). *Diabet Med,* 18**:** 178-184, 2001 10.1046/j.1464-5491.2001.00458.x
16. Ponto KA, Koenig J, Peto T, Lamparter J, Raum P, Wild PS, et al.: Prevalence of diabetic retinopathy in screening-detected diabetes mellitus: results from the

Gutenberg Health Study (GHS). *Diabetologia,* 59**:** 1913-1919, 2016 10.1007/s00125-016-4013-5
17. Lai AK, Lo AC: Animal models of diabetic retinopathy: summary and comparison. *J Diabetes Res,* 2013**:** 106594, 2013 10.1155/2013/106594
18. Olivares AM, Althoff K, Chen GF, Wu S, Morrisson MA, DeAngelis MM, et al.: Animal Models of Diabetic Retinopathy. *Curr Diab Rep,* 17**:** 93, 2017 10.1007/s11892-017-0913-0
19. Wu KK, Huan Y: Streptozotocin-induced diabetic models in mice and rats. *Curr Protoc Pharmacol,* Chapter 5**:** Unit 5 47, 2008 10.1002/0471141755.ph0547s40
20. Feit-Leichman RA, Kinouchi R, Takeda M, Fan Z, Mohr S, Kern TS, et al.: Vascular damage in a mouse model of diabetic retinopathy: relation to neuronal and glial changes. *Invest Ophthalmol Vis Sci,* 46**:** 4281-4287, 2005 10.1167/iovs.04-1361
21. Martin PM, Roon P, Van Ells TK, Ganapathy V, Smith SB: Death of retinal neurons in streptozotocin-induced diabetic mice. *Invest Ophthalmol Vis Sci,* 45**:** 3330-3336, 2004 10.1167/iovs.04-0247
22. Intine RV, Olsen AS, Sarras MP, Jr.: A zebrafish model of diabetes mellitus and metabolic memory. *J Vis Exp***:** e50232, 2013 10.3791/50232
23. Robinson R, Barathi VA, Chaurasia SS, Wong TY, Kern TS: Update on animal models of diabetic retinopathy: from molecular approaches to mice and higher mammals. *Dis Model Mech,* 5**:** 444-456, 2012 10.1242/dmm.009597
24. Gleeson M, Connaughton V, Arneson LS: Induction of hyperglycaemia in zebrafish (Danio rerio) leads to morphological changes in the retina. *Acta Diabetol,* 44**:** 157-163, 2007 10.1007/s00592-007-0257-3
25. Wang J, Takeuchi T, Tanaka S, Kubo SK, Kayo T, Lu D, et al.: A mutation in the insulin 2 gene induces diabetes with severe pancreatic beta-cell dysfunction in the Mody mouse. *J Clin Invest,* 103**:** 27-37, 1999 10.1172/JCI4431
26. Leiter EH, Prochazka M, Coleman DL: The non-obese diabetic (NOD) mouse. *Am J Pathol,* 128**:** 380-383, 1987
27. Yoon JW, Leiter EH, Coleman DL, Kim MK, Pak CY, McArthur RG, et al.: Genetic control of organ-reactive autoantibody production in mice by obesity (ob) diabetes (db) genes. *Diabetes,* 37**:** 1287-1293, 1988 10.2337/diab.37.9.1287
28. Kern TS, Antonetti DA, Smith LEH: Pathophysiology of Diabetic Retinopathy: Contribution and Limitations of Laboratory Research. *Ophthalmic Res,* 62**:** 196-202, 2019 10.1159/000500026
29. Kim CB, D'Amore PA, Connor KM: Revisiting the mouse model of oxygen-induced retinopathy. *Eye Brain,* 8**:** 67-79, 2016 10.2147/EB.S94447
30. Stahl A, Connor KM, Sapieha P, Chen J, Dennison RJ, Krah NM, et al.: The mouse retina as an angiogenesis model. *Invest Ophthalmol Vis Sci,* 51**:** 2813-2826, 2010 10.1167/iovs.10-5176
31. Wiggenhauser LM, Qi H, Stoll SJ, Metzger L, Bennewitz K, Poschet G, et al.: Activation of Retinal Angiogenesis in Hyperglycemic pdx1 (-/-) Zebrafish Mutants. *Diabetes,* 69**:** 1020-1031, 2020 10.2337/db19-0873
32. Bloodworth JM, Jr.: Diabetic retinopathy. *Diabetes,* 11**:** 1-22, 1962
33. Hammes HP, Federoff HJ, Brownlee M: Nerve growth factor prevents both neuroretinal programmed cell death and capillary pathology in experimental diabetes. *Mol Med,* 1**:** 527-534, 1995
34. Barber AJ, Lieth E, Khin SA, Antonetti DA, Buchanan AG, Gardner TW: Neural apoptosis in the retina during experimental and human diabetes. Early onset and effect of insulin. *J Clin Invest,* 102**:** 783-791, 1998 10.1172/JCI2425

35. Lieth E, Gardner TW, Barber AJ, Antonetti DA, Penn State Retina Research G: Retinal neurodegeneration: early pathology in diabetes. *Clin Exp Ophthalmol,* 28**:** 3-8, 2000 10.1046/j.1442-9071.2000.00222.x
36. Park SH, Park JW, Park SJ, Kim KY, Chung JW, Chun MH, et al.: Apoptotic death of photoreceptors in the streptozotocin-induced diabetic rat retina. *Diabetologia,* 46**:** 1260-1268, 2003 10.1007/s00125-003-1177-6
37. Iadecola C: Neurovascular regulation in the normal brain and in Alzheimer's disease. *Nat Rev Neurosci,* 5**:** 347-360, 2004 10.1038/nrn1387
38. Hawkins BT, Davis TP: The blood-brain barrier/neurovascular unit in health and disease. *Pharmacol Rev,* 57**:** 173-185, 2005 10.1124/pr.57.2.4
39. Metea MR, Newman EA: Signalling within the neurovascular unit in the mammalian retina. *Exp Physiol,* 92**:** 635-640, 2007 10.1113/expphysiol.2006.036376
40. Pemp B, Garhofer G, Weigert G, Karl K, Resch H, Wolzt M, et al.: Reduced retinal vessel response to flicker stimulation but not to exogenous nitric oxide in type 1 diabetes. *Invest Ophthalmol Vis Sci,* 50**:** 4029-4032, 2009 10.1167/iovs.08-3260
41. Lott ME, Slocomb JE, Shivkumar V, Smith B, Gabbay RA, Quillen D, et al.: Comparison of retinal vasodilator and constrictor responses in type 2 diabetes. *Acta Ophthalmol,* 90**:** e434-441, 2012 10.1111/j.1755-3768.2012.02445.x
42. Simo R, Sundstrom JM, Antonetti DA: Ocular Anti-VEGF therapy for diabetic retinopathy: the role of VEGF in the pathogenesis of diabetic retinopathy. *Diabetes Care,* 37**:** 893-899, 2014 10.2337/dc13-2002
43. Sone H, Kawakami Y, Okuda Y, Kondo S, Hanatani M, Suzuki H, et al.: Vascular endothelial growth factor is induced by long-term high glucose concentration and up-regulated by acute glucose deprivation in cultured bovine retinal pigmented epithelial cells. *Biochem Biophys Res Commun,* 221**:** 193-198, 1996 10.1006/bbrc.1996.0568
44. Lu M, Kuroki M, Amano S, Tolentino M, Keough K, Kim I, et al.: Advanced glycation end products increase retinal vascular endothelial growth factor expression. *J Clin Invest,* 101**:** 1219-1224, 1998 10.1172/JCI1277
45. Park DY, Lee J, Kim J, Kim K, Hong S, Han S, et al.: Plastic roles of pericytes in the blood-retinal barrier. *Nat Commun,* 8**:** 15296, 2017 10.1038/ncomms15296
46. Geraldes P, Hiraoka-Yamamoto J, Matsumoto M, Clermont A, Leitges M, Marette A, et al.: Activation of PKC-delta and SHP-1 by hyperglycemia causes vascular cell apoptosis and diabetic retinopathy. *Nat Med,* 15**:** 1298-1306, 2009 10.1038/nm.2052
47. Duh EJ, Sun JK, Stitt AW: Diabetic retinopathy: current understanding, mechanisms, and treatment strategies. *JCI Insight,* 2, 2017 10.1172/jci.insight.93751
48. Simo R, Stitt AW, Gardner TW: Neurodegeneration in diabetic retinopathy: does it really matter? *Diabetologia,* 61**:** 1902-1912, 2018 10.1007/s00125-018-4692-1
49. Bringmann A, Wiedemann P: Muller glial cells in retinal disease. *Ophthalmologica,* 227**:** 1-19, 2012 10.1159/000328979
50. Reichenbach A, Bringmann A: Glia of the human retina. *Glia,* 68**:** 768-796, 2020 10.1002/glia.23727
51. Heckler K, Kroll J: Zebrafish as a Model for the Study of Microvascular Complications of Diabetes and Their Mechanisms. *Int J Mol Sci,* 18, 2017 10.3390/ijms18092002
52. Kimmel CB, Ballard WW, Kimmel SR, Ullmann B, Schilling TF: Stages of embryonic development of the zebrafish. *Dev Dyn,* 203**:** 253-310, 1995 10.1002/aja.1002030302

53. Amsterdam A, Becker TS: Transgenes as screening tools to probe and manipulate the zebrafish genome. *Dev Dyn,* 234**:** 255-268, 2005 10.1002/dvdy.20541
54. Gut P, Reischauer S, Stainier DYR, Arnaout R: Little Fish, Big Data: Zebrafish as a Model for Cardiovascular and Metabolic Disease. *Physiol Rev,* 97**:** 889-938, 2017 10.1152/physrev.00038.2016
55. Howe K, Clark MD, Torroja CF, Torrance J, Berthelot C, Muffato M, et al.: The zebrafish reference genome sequence and its relationship to the human genome. *Nature,* 496**:** 498-503, 2013 10.1038/nature12111
56. Jinek M, Chylinski K, Fonfara I, Hauer M, Doudna JA, Charpentier E: A programmable dual-RNA-guided DNA endonuclease in adaptive bacterial immunity. *Science,* 337**:** 816-821, 2012 10.1126/science.1225829
57. Meier A, Nelson R, Connaughton VP: Color Processing in Zebrafish Retina. *Front Cell Neurosci,* 12**:** 327, 2018 10.3389/fncel.2018.00327
58. Bilotta J, Saszik S: The zebrafish as a model visual system. *Int J Dev Neurosci,* 19**:** 621-629, 2001 10.1016/s0736-5748(01)00050-8
59. Alvarez Y, Cederlund ML, Cottell DC, Bill BR, Ekker SC, Torres-Vazquez J, et al.: Genetic determinants of hyaloid and retinal vasculature in zebrafish. *BMC Dev Biol,* 7**:** 114, 2007 10.1186/1471-213X-7-114
60. Fruttiger M: Development of the retinal vasculature. *Angiogenesis,* 10**:** 77-88, 2007 10.1007/s10456-007-9065-1
61. Middel CS, Hammes HP, Kroll J: Advancing Diabetic Retinopathy Research: Analysis of the Neurovascular Unit in Zebrafish. *Cells,* 10, 2021 10.3390/cells10061313
62. Marin-Juez R, Jong-Raadsen S, Yang S, Spaink HP: Hyperinsulinemia induces insulin resistance and immune suppression via Ptpn6/Shp1 in zebrafish. *J Endocrinol,* 222**:** 229-241, 2014 10.1530/JOE-14-0178
63. Planas JV, Capilla E, Gutierrez J: Molecular identification of a glucose transporter from fish muscle. *FEBS Lett,* 481**:** 266-270, 2000 10.1016/s0014-5793(00)02020-2
64. Maddison LA, Joest KE, Kammeyer RM, Chen W: Skeletal muscle insulin resistance in zebrafish induces alterations in beta-cell number and glucose tolerance in an age- and diet-dependent manner. *Am J Physiol Endocrinol Metab,* 308**:** E662-669, 2015 10.1152/ajpendo.00441.2014
65. Tehrani Z, Lin S: Endocrine pancreas development in zebrafish. *Cell Cycle,* 10**:** 3466-3472, 2011 10.4161/cc.10.20.17764
66. Zang L, Maddison LA, Chen W: Zebrafish as a Model for Obesity and Diabetes. *Front Cell Dev Biol,* 6**:** 91, 2018 10.3389/fcell.2018.00091
67. Al-Quobaili F, Montenarh M: Pancreatic duodenal homeobox factor-1 and diabetes mellitus type 2 (review). *Int J Mol Med,* 21**:** 399-404, 2008
68. Liu T, Wang CY, Yu F, Gou SM, Wu HS, Xiong JX, et al.: In vitro pancreas duodenal homeobox-1 enhances the differentiation of pancreatic ductal epithelial cells into insulin-producing cells. *World J Gastroenterol,* 13**:** 5232-5237, 2007 10.3748/wjg.v13.i39.5232
69. Stoffers DA, Ferrer J, Clarke WL, Habener JF: Early-onset type-II diabetes mellitus (MODY4) linked to IPF1. *Nat Genet,* 17**:** 138-139, 1997 10.1038/ng1097-138
70. Sachdeva MM, Claiborn KC, Khoo C, Yang J, Groff DN, Mirmira RG, et al.: Pdx1 (MODY4) regulates pancreatic beta cell susceptibility to ER stress. *Proc Natl Acad Sci U S A,* 106**:** 19090-19095, 2009 10.1073/pnas.0904849106
71. Milewski WM, Duguay SJ, Chan SJ, Steiner DF: Conservation of PDX-1 structure, function, and expression in zebrafish. *Endocrinology,* 139**:** 1440-1449, 1998 10.1210/endo.139.3.5768

72. Kimmel RA, Dobler S, Schmitner N, Walsen T, Freudenblum J, Meyer D: Diabetic pdx1-mutant zebrafish show conserved responses to nutrient overload and anti-glycemic treatment. *Scientific Reports,* 5, 2015 10.1038/srep14241
73. Ali Z, Zang J, Lagali N, Schmitner N, Salvenmoser W, Mukwaya A, et al.: Photoreceptor Degeneration Accompanies Vascular Changes in a Zebrafish Model of Diabetic Retinopathy. *Invest Ophthalmol Vis Sci,* 61**:** 43, 2020 10.1167/iovs.61.2.43
74. Koepsell H: Glucose transporters in brain in health and disease. *Pflugers Arch,* 472**:** 1299-1343, 2020 10.1007/s00424-020-02441-x
75. Lawson ND, Weinstein BM: In vivo imaging of embryonic vascular development using transgenic zebrafish. *Dev Biol,* 248**:** 307-318, 2002 10.1006/dbio.2002.0711
76. Blum Y, Belting HG, Ellertsdottir E, Herwig L, Luders F, Affolter M: Complex cell rearrangements during intersegmental vessel sprouting and vessel fusion in the zebrafish embryo. *Dev Biol,* 316**:** 312-322, 2008 10.1016/j.ydbio.2008.01.038
77. Wohlfart DP, Lou B, Middel CS, Morgenstern J, Fleming T, Sticht C, et al.: Accumulation of acetaldehyde in aldh2.1(-/-) zebrafish causes increased retinal angiogenesis and impaired glucose metabolism. *Redox Biol,* 50**:** 102249, 2022 10.1016/j.redox.2022.102249
78. Wilson JM, Bunte RM, Carty AJ: Evaluation of rapid cooling and tricaine methanesulfonate (MS222) as methods of euthanasia in zebrafish (Danio rerio). *J Am Assoc Lab Anim Sci,* 48**:** 785-789, 2009
79. Zang L, Shimada Y, Nishimura Y, Tanaka T, Nishimura N: Repeated Blood Collection for Blood Tests in Adult Zebrafish. *J Vis Exp***:** e53272, 2015 10.3791/53272
80. Wiggenhauser LM, Kohl K, Dietrich N, Hammes HP, Kroll J: Studying Diabetes Through the Eyes of a Fish: Microdissection, Visualization, and Analysis of the Adult tg(fli:EGFP) Zebrafish Retinal Vasculature. *J Vis Exp*, 2017 10.3791/56674
81. Busch S, Kannt A, Kolibabka M, Schlotterer A, Wang Q, Lin J, et al.: Systemic treatment with erythropoietin protects the neurovascular unit in a rat model of retinal neurodegeneration. *PLoS One,* 9**:** e102013, 2014 10.1371/journal.pone.0102013
82. Patton J, Kent M, Kara N: Inhibition of GABAA-ρ receptors induces retina regeneration in zebrafish. *Neural Regeneration Research,* 16, 2021 10.4103/1673-5374.286972
83. Dietrich N, Hammes HP: Retinal digest preparation: a method to study diabetic retinopathy. *Methods Mol Biol,* 933**:** 291-302, 2012 10.1007/978-1-62703-068-7_19
84. Hill JT, Demarest BL, Bisgrove BW, Su YC, Smith M, Yost HJ: Poly peak parser: Method and software for identification of unknown indels using sanger sequencing of polymerase chain reaction products. *Dev Dyn,* 243**:** 1632-1636, 2014 10.1002/dvdy.24183
85. Fraher D, Sanigorski A, Mellett NA, Meikle PJ, Sinclair AJ, Gibert Y: Zebrafish Embryonic Lipidomic Analysis Reveals that the Yolk Cell Is Metabolically Active in Processing Lipid. *Cell Rep,* 14**:** 1317-1329, 2016 10.1016/j.celrep.2016.01.016
86. Menke AL, Spitsbergen JM, Wolterbeek AP, Woutersen RA: Normal anatomy and histology of the adult zebrafish. *Toxicol Pathol,* 39**:** 759-775, 2011 10.1177/0192623311409597

87. Ando K, Fukuhara S, Izumi N, Nakajima H, Fukui H, Kelsh RN, et al.: Clarification of mural cell coverage of vascular endothelial cells by live imaging of zebrafish. *Development,* 143**:** 1328-1339, 2016 10.1242/dev.132654
88. Lodd E, Wiggenhauser LM, Morgenstern J, Fleming TH, Poschet G, Buttner M, et al.: The combination of loss of glyoxalase1 and obesity results in hyperglycemia. *JCI Insight,* 4, 2019 10.1172/jci.insight.126154
89. Olsen AS, Sarras MP, Jr., Intine RV: Limb regeneration is impaired in an adult zebrafish model of diabetes mellitus. *Wound Repair Regen,* 18**:** 532-542, 2010 10.1111/j.1524-475X.2010.00613.x
90. Tanvir Z, Nelson RF, DeCicco-Skinner K, Connaughton VP: One month of hyperglycemia alters spectral responses of the zebrafish photopic electroretinogram. *Dis Model Mech,* 11, 2018 10.1242/dmm.035220
91. Goldman D: Muller glial cell reprogramming and retina regeneration. *Nat Rev Neurosci,* 15**:** 431-442, 2014 10.1038/nrn3723
92. Lenkowski JR, Raymond PA: Muller glia: Stem cells for generation and regeneration of retinal neurons in teleost fish. *Prog Retin Eye Res,* 40**:** 94-123, 2014 10.1016/j.preteyeres.2013.12.007
93. Gorsuch RA, Hyde DR: Regulation of Muller glial dependent neuronal regeneration in the damaged adult zebrafish retina. *Exp Eye Res,* 123**:** 131-140, 2014 10.1016/j.exer.2013.07.012
94. Kassen SC, Ramanan V, Montgomery JE, C TB, Liu CG, Vihtelic TS, et al.: Time course analysis of gene expression during light-induced photoreceptor cell death and regeneration in albino zebrafish. *Dev Neurobiol,* 67**:** 1009-1031, 2007 10.1002/dneu.20362
95. Powell C, Grant AR, Cornblath E, Goldman D: Analysis of DNA methylation reveals a partial reprogramming of the Muller glia genome during retina regeneration. *Proc Natl Acad Sci U S A,* 110**:** 19814-19819, 2013 10.1073/pnas.1312009110
96. Nagashima M, Barthel LK, Raymond PA: A self-renewing division of zebrafish Muller glial cells generates neuronal progenitors that require N-cadherin to regenerate retinal neurons. *Development,* 140**:** 4510-4521, 2013 10.1242/dev.090738
97. Rao MB, Didiano D, Patton JG: Neurotransmitter-Regulated Regeneration in the Zebrafish Retina. *Stem Cell Reports,* 8**:** 831-842, 2017 10.1016/j.stemcr.2017.02.007
98. Coughlin BA, Feenstra DJ, Mohr S: Muller cells and diabetic retinopathy. *Vision Res,* 139**:** 93-100, 2017 10.1016/j.visres.2017.03.013
99. Poitry-Yamate CL, Poitry S, Tsacopoulos M: Lactate released by Muller glial cells is metabolized by photoreceptors from mammalian retina. *J Neurosci,* 15**:** 5179-5191, 1995
100. Kumagai AK, Glasgow BJ, Pardridge WM: GLUT1 glucose transporter expression in the diabetic and nondiabetic human eye. *Invest Ophthalmol Vis Sci,* 35**:** 2887-2894, 1994
101. Ludvigson MA, Sorenson RL: Immunohistochemical localization of aldose reductase. II. Rat eye and kidney. *Diabetes,* 29**:** 450-459, 1980 10.2337/diab.29.6.450
102. Newman E, Reichenbach A: The Muller cell: a functional element of the retina. *Trends Neurosci,* 19**:** 307-312, 1996 10.1016/0166-2236(96)10040-0
103. Gerhardinger C, Costa MB, Coulombe MC, Toth I, Hoehn T, Grosu P: Expression of acute-phase response proteins in retinal Muller cells in diabetes. *Invest Ophthalmol Vis Sci,* 46**:** 349-357, 2005 10.1167/iovs.04-0860

104. Mizutani M, Gerhardinger C, Lorenzi M: Muller cell changes in human diabetic retinopathy. *Diabetes,* 47**:** 445-449, 1998 10.2337/diabetes.47.3.445
105. Mitchell DM, Lovel AG, Stenkamp DL: Dynamic changes in microglial and macrophage characteristics during degeneration and regeneration of the zebrafish retina. *J Neuroinflammation,* 15**:** 163, 2018 10.1186/s12974-018-1185-6
106. Buschini E, Piras A, Nuzzi R, Vercelli A: Age related macular degeneration and drusen: neuroinflammation in the retina. *Prog Neurobiol,* 95**:** 14-25, 2011 10.1016/j.pneurobio.2011.05.011
107. Zeng HY, Green WR, Tso MO: Microglial activation in human diabetic retinopathy. *Arch Ophthalmol,* 126**:** 227-232, 2008 10.1001/archophthalmol.2007.65
108. Caceres L, Prykhozhij SV, Cairns E, Gjerde H, Duff NM, Collett K, et al.: Frizzled 4 regulates ventral blood vessel remodeling in the zebrafish retina. *Dev Dyn,* 248**:** 1243-1256, 2019 10.1002/dvdy.117
109. Alvarez Y, Astudillo O, Jensen L, Reynolds AL, Waghorne N, Brazil DP, et al.: Selective inhibition of retinal angiogenesis by targeting PI3 kinase. *PLoS One,* 4**:** e7867, 2009 10.1371/journal.pone.0007867
110. Hartmann DA, Underly RG, Grant RI, Watson AN, Lindner V, Shih AY: Pericyte structure and distribution in the cerebral cortex revealed by high-resolution imaging of transgenic mice. *Neurophotonics,* 2**:** 041402, 2015 10.1117/1.NPh.2.4.041402
111. Gardiner TA, Archer DB, Curtis TM, Stitt AW: Arteriolar involvement in the microvascular lesions of diabetic retinopathy: implications for pathogenesis. *Microcirculation,* 14**:** 25-38, 2007 10.1080/10739680601072123
112. vom Hagen F, Feng Y, Hillenbrand A, Hoffmann S, Shani M, Deutsch U, et al.: Early loss of arteriolar smooth muscle cells: more than just a pericyte loss in diabetic retinopathy. *Exp Clin Endocrinol Diabetes,* 113**:** 573-576, 2005 10.1055/s-2005-872894
113. Ando K, Shih YH, Ebarasi L, Grosse A, Portman D, Chiba A, et al.: Conserved and context-dependent roles for pdgfrb signaling during zebrafish vascular mural cell development. *Dev Biol,* 479**:** 11-22, 2021 10.1016/j.ydbio.2021.06.010
114. Wang Y, Pan L, Moens CB, Appel B: Notch3 establishes brain vascular integrity by regulating pericyte number. *Development,* 141**:** 307-317, 2014 10.1242/dev.096107
115. Santoro MM, Pesce G, Stainier DY: Characterization of vascular mural cells during zebrafish development. *Mech Dev,* 126**:** 638-649, 2009 10.1016/j.mod.2009.06.1080
116. Wiggenhauser LM, Metzger L, Bennewitz K, Soleymani S, Boger M, Tabler CT, et al.: pdx1 Knockout Leads to a Diabetic Nephropathy-Like Phenotype in Zebrafish and Identifies Phosphatidylethanolamine as Metabolite Promoting Early Diabetic Kidney Damage. *Diabetes*, 2022 10.2337/db21-0645

8 SUPPLEMENTARY MATERIAL

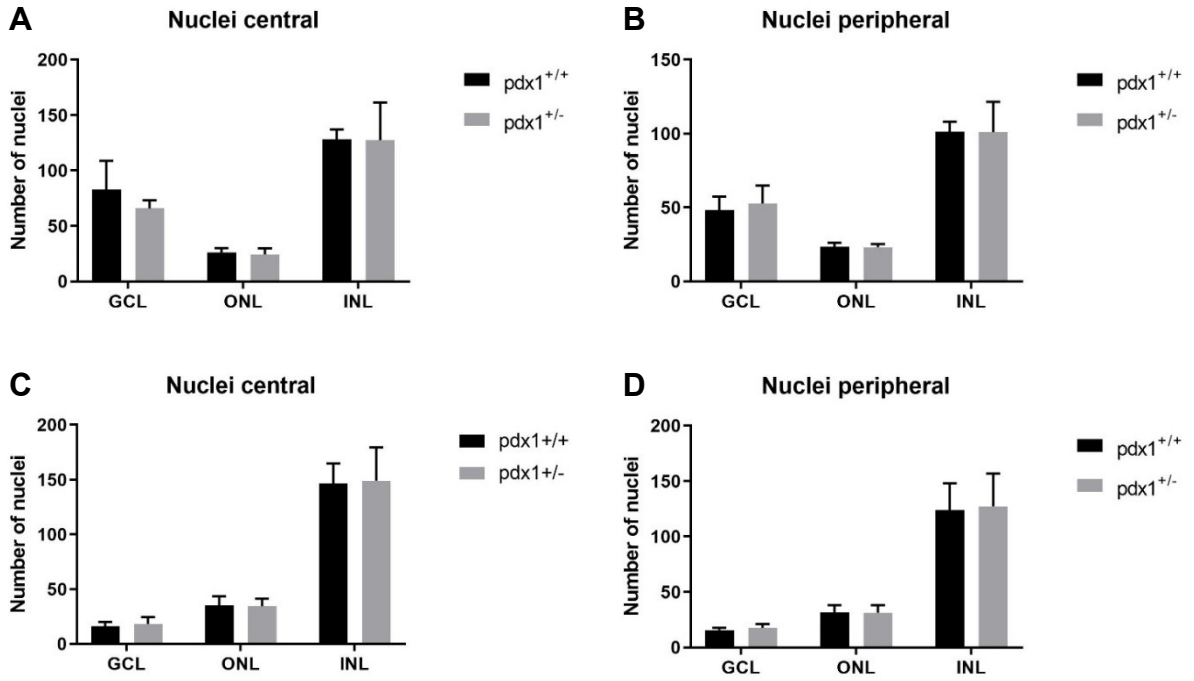

Supplementary figure 1: *pdx1*$^{+/-}$ mutants do not exhibit fewer neuronal nuclei at any point. A and B) Neuronal nuclei in *pdx1*$^{+/-}$ zebrafish (n=6) and their littermates (n=5) at 12 mpf. E and F) Neuronal nuclei in *pdx1*$^{+/-}$ zebrafish (n=6) and their littermates (n=4) at 21 mpf.

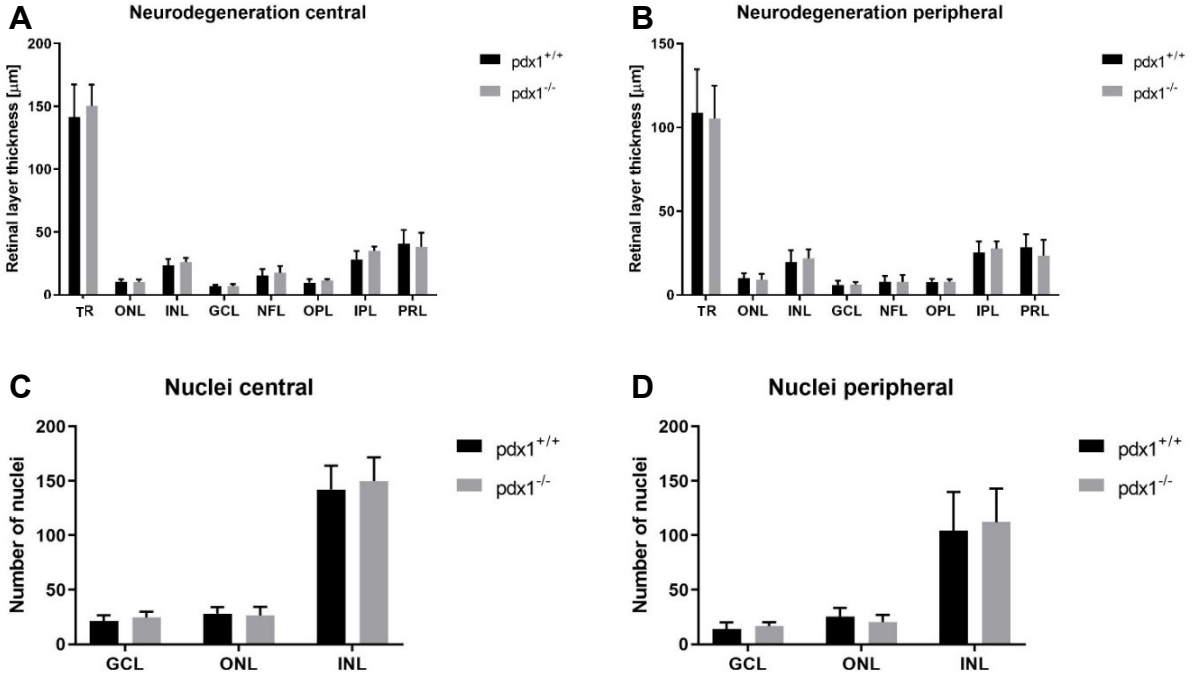

Supplementary figure 2: *pdx1*$^{-/-}$ mutants do not show signs of neurodegeneration at 18mpf. A and B) Retinal layer thickness in *pdx1*$^{-/-}$ zebrafish (n=5) and their littermates (n=5). C and D) Nuclei numbers in *pdx1*$^{-/-}$ zebrafish (n=5) and their littermates (n=5).

9 PUBLICATIONS

2021 **Middel CS,** Hammes HP, Kroll J: Advancing Diabetic Retinopathy Research: Analysis of the Neurovascular Unit in Zebrafish. *Cells,* 10, 2021 10.3390/cells10061313

2022 Wohlfart DP, Lou B, **Middel CS**, Morgenstern J, Fleming T, Sticht C, et al.: Accumulation of acetaldehyde in aldh2.1(-/-) zebrafish causes increased retinal angiogenesis and impaired glucose metabolism. *Redox Biol,* 50**:** 102249, 2022 10.1016/j.redox.2022.102249

10 LEBENSLAUF

PERSONALIEN

Name und Vorname:	Chiara Simone Middel
Geburtsdatum:	17.10.1997
Geburtsort:	Darmstadt

SCHULISCHER WERDEGANG

07/2003 – 06/2007	Heinrich-Hoffmann-Grundschule Darmstadt
07/2007 – 06/2015	Edith-Stein-Schule Darmstadt
11.06.2015	Abitur, Note 1,0

UNIVERSITÄRER WERDEGANG

WS 2016/17	Beginn des Studiums der Humanmedizin an der Medizinischen Fakultät Mannheim der Universität Heidelberg
10.09.2018	Erster Abschnitt der Ärztlichen Prüfung, Note 2,0
2018 – 2022	Hauptstudium
08.04.2022	Zweiter Abschnitt der Ärztlichen Prüfung, Note 2,0
2022 – 2023	Praktisches Jahr
Voraussichtlich 2023	Dritter Abschnitt der Ärztlichen Prüfung

11 DANKSAGUNG

Zunächst möchte ich Herrn Professor Doktor Jens Kroll für die Überlassung des Themas und für die großartige Betreuung danken. Insbesondere Ihre ständige Erreichbarkeit und Bereitschaft, Unterstützung zu leisten und neue Ergebnisse gemeinsam zu interpretieren und zu diskutieren haben mir sehr geholfen. Unsere Gespräche haben mich stets motiviert, noch ein kleines bisschen mehr aus dem Thema herauszuholen.

Als nächstes möchte ich Herrn Professor Doktor Hans-Peter Hammes für die exzellente Ko-Betreuung danken. Ohne die bereitwillige Aufnahme in Ihr Team und die stete Unterstützung hätte ich das Thema nicht so umfänglich verstehen und ausarbeiten können. Die geführten Diskussionen haben mir stets geholfen, das Thema und meine wissenschaftliche Arbeit zu vertiefen und weiterzuentwickeln.

Nadine Dietrich möchte ich von Herzen für die geduldige Unterstützung bei den Versuchen und die schönen Gespräche (sowohl über die Arbeit als auch über Privates) danken. Ohne die Unterstützung wäre die Hälfte der Versuche schief gegangen, oder hätte zumindest dreimal so lange gedauert.

Ich danke Katrin Bennewitz für die tatkräftige Unterstützung, wann immer ich sie benötigt habe, und die Einführung in die Arbeit mit den Zebrafischen; ohne dich wäre diese Arbeit nicht möglich gewesen.

Mein herzlicher Dank gehört Frau Dr. Nadine Volk und Nina Wilhelm von der Gewebebank am Pathologischen Institut Heidelberg, die die Antikörper-Färbungen etabliert und mir die gefärbten Schnitte zur Auswertung gegeben haben.

Ich danke Mike Boger für die gute Zusammenarbeit als Graduiertenvertretung im Graduiertenkolleg DIAMICOM und für die tatkräftige Unterstützung bei meinen Experimenten. Lena Metzger danke ich für die gute Zusammenarbeit mit den *pdx1*$^{+/-}$ Zebrafischen und für die Unterstützung, von der ich stark profitieren konnte. Lucas Moritz Wiggenhauser danke ich für die Vorarbeit und die Etablierung der *pdx1*$^{+/-}$ Zebrafischlinie.

Ich möchte allen Kolleg:innen der AG Kroll für die gute Zusammenarbeit und die schöne gemeinsame Zeit danken: David Wohlfart, Christoph Tabler, Bowen Lou, Haozhe Qi, Xiaogang Li und Björn Hühn.

Ebenso möchte ich allen Kolleg:innen der AG Hammes für die gute Zusammenarbeit danken: Luke Kurowski, Dr. Andrea Schlotterer, Dr. Jihong Lin, Dr. Ying Chen, Tina Jung und Jacqueline Raum. Insbesondere geht mein Dank auch an Katharina Murillo für die vielen Tipps und die netten Gespräche.

Diese Arbeit wäre ohne Förderung der Deutschen Forschungsgemeinschaft (DFG) im Rahmen des Graduiertenkollegs DIAMICOM (IRTG 1874/2) nicht möglich gewesen. Ich bedanke mich für die Unterstützung bei der Core Facility Live Cell Imaging Mannheim (LiMa) am CBTM (DFG INST 91027/9-1 FUGG).

Zuletzt danke ich meinen Freunden und meiner Familie, deren Unterstützung während der letzten Jahre unersetzlich war.